Late Neogene nannofossil assemblages as tracers of ocean circulation and paleoproductivity over the NW Australian shelf

Boris-Theofanis Karatsolis[1] and Jorijntje Henderiks[1]

[1]Department of Earth Sciences, Uppsala University, Uppsala, 752 36, Sweden

5   *Correspondence to*: Boris Theofanis Karatsolis (boris.karatsolis@geo.uu.se)

Abstract.

Late Miocene to Pliocene sediments from the NW Australian shelf, drilled by the International Ocean Discovery Program (IODP) Expedition 356, provide unique records of paleoclimatic variations under warmer-than-present conditions. ~~Recent investigations of sediments recovered from the shelf during International Ocean Discovery Program (IODP) Expedition 356, have produced a number of well-dated time-series that cover the late Neogene and can therefore assist with more detailed reconstructions.~~During the period from 6-3.5 million years ago (Ma), the area was dominated by warm, tropical waters supplied by an intensified, uninterrupted Indonesian Throughflow and characterised by prevailing humid conditions, ~~as well as~~including ~~and~~ increased precipitation and river runoff. Despite the available information regarding the general paleoclimatic conditions, little is known about the concurrent regional ocean circulation patterns and the relative ~~intensity~~strength of seasonally flowing boundary currents, such as the Leeuwin Current. ~~Recent investigations of sediments recovered from the shelf during International Ocean Discovery Program (IODP) Expedition 356, have produced a number of well-dated time-series that cover the late Neogene and can therefore assist with more detailed reconstructions.~~In this study, we investigate two astronomically-tuned calcareous nannofossil ~~records~~time series from IODP Sites U1463 and U1464 ~~that can help us trace and understand~~to track long-term changes in ocean circulation and water column stratification~~seasonality~~, as well as their effect ~~on~~which influences the ~~nutrient replenishment~~availability of nutrients in the upper photic zone and is considered a primary control on the (paleo)productivity of marine phytoplankton. By ~~looking into~~documenting shifts in the dominant species within the nannofossil ~~assemblage, and~~assemblages and comparing ~~them~~these ~~with~~to paleotemperature gradients between the NW Australian shelf and the eastern Indian Ocean, we identify ~~the main periods of change in stratification and nutrient availability that occurred over the continental shelf. Our results indicate~~ a significant change in ecological and oceanographic regime that occurred across the Miocene~~ to~~-Pliocene boundary (5.4–5.2 Ma), which can be attributed to an ~~increase in seasonality and~~ an overall intensification of the upper water column mixing over the shelf. ~~Major changes~~ Significant changes in nannofossil abundance and species ~~distribution~~composition ~~and abundances in the nannofossil assemblages~~ that reflect broader-scale processes and evolutionary events, such as ~~the extinction of *Sphenolithus* spp. (~3.54 Ma) and~~ the termination of the late Miocene to early Pliocene biogenic bloom in the eastern Indian Ocean (4.6-4.4 Ma) and the extinction of *Sphenolithus* spp. (~3.54 Ma), occurred long after this regional regime shift.

1 Introduction

Calcareous nannoplankton (including coccolithophores) ~~Marine phytoplankton~~ are sensitive indicators of ~~current and~~ current and past climatic change, ~~with coccolithophores being the most extensively studied, because o~~because as primary producers, they are primarily dependent on the prevailing (and seasonally changing) physicochemical conditions, such as nutrient availability and temperature, within the upper sunlit layers of the ocean. The abundant and well-preserved fossil record of their calcareous platelets (calcareous nannofossils) in shallow marine and deep-sea sediments has been used to reconstruct f ~~due to their long, abundant, and mostly well-preserved record of their fossilised calcareous platelets (calcareous nannofossils) in shallow marine and deep sea sediments since the late Triassic. Through their fossilised calcareous platelets (coccoliths and nannoliths), Due to this characteristic, these organisms~~ have the potential to record both regional paleoclimatic and paleoceanographic changes, but also global processes such as evolution (speciation and extinction) and basin-wide changes in ocean chemistry (Beaufort et al., 1997; Bolton et al., 2016; O'Dea et al., 2014; Thierstein and Young, 2004). Because of ~~this~~the interplay of regional and global ~~signals~~imprints preserved in the sediment~~ary~~ record, nannofossil assemblage studies come with a set of challenges, especially in highly dynamic environments across continental shelves. In such areas, calcareous nannoplankton~~coccolithophore~~ communities may be significantly different ~~than~~from open ocean marine settings, owing to the influence ~~from~~of parameters such as seasonal water column stratification and tidal mixing (Sharples et al., 2009; Van Oostende et al., 2012), as well as variations in river runoff and nutrient input (Harlay et al., 2010; Poulton et al., 2014). This further complicates the task of using ~~the~~ nannofossil assemblage~~s~~ to consistently differentiate between signals of regional paleoclimatic forcing and broad-scale evolutionary trends and changes in the ocean's nutrient ==availability==budget.

The NW Australian shelf serves as an important test-case to try and tackle these challenges, because of its position within the dynamic climate system of the Indo-Pacific warm pool and near the only remaining "equatorial warm water valve". Modern ocean circulation in the area is controlled by a variation in intensity of the Indonesian Throughflow (ITF) and the Leeuwin Current (LC). The ITF is the warm surface current that transports water from the Western Pacific Warm Pool (WPWP) into the Indian Ocean (Du and Qu, 2010; Gordon et al., 1997; Figure 1). The LC is a boundary current that is sourced by the ITF and transports warm water southwards (Figure 1), with significant implications for fisheries and the persistence of tropical biota in the high latitudes of western and southwestern Australia (e.g. Kendrick et al., 2009 and references therein). Its strength varies seasonally, with the strongest flow being observed during austral winter, when latitudinal steric height gradients are steeper (e.g. Godfrey and Ridgway, 1985; Ridgway and Godfrey, 2015). Interannually, stronger/~~(weaker)~~ LC is linked to La Niña/~~(El Niño)~~ conditions, with a mean annual transported volume of 4.2 Sv/~~(3 Sv)~~ (e.g., Feng et al., 2003, 2009). Additionally, this flow is known to consist of warm-core anticyclonic eddies that can promote phytoplankton production across the western Australian shelf (Koslow et al., 2008; Thompson et al., 2007). The NW Australian shelf is a source area of the LC, contributing to its total volume through a surface current called the Holloway Current (HC; D'Adamo et al., 2009; Holloway

and Nye, 1985), that flows south-westward along the shelf. Weak upwelling events have been observed in the area both during summer and winter months, when westerly winds are strong enough to overcome the steric height gradient (Holloway and Nye, 1985). Modern observational data and forecasts (E.U. Copernicus Marine Service Information) show that during austral winter, when the LC is strong, the NW Australian shelf area is characterised by a mixed layer deepening, which reaches ~100m and occurs because of an invigoration of the upper water column mixing. At the same time, chlorophyll-a increases in the surface layer, driven by an increase in water column cooling and advective mixing (Figures 2, 3).
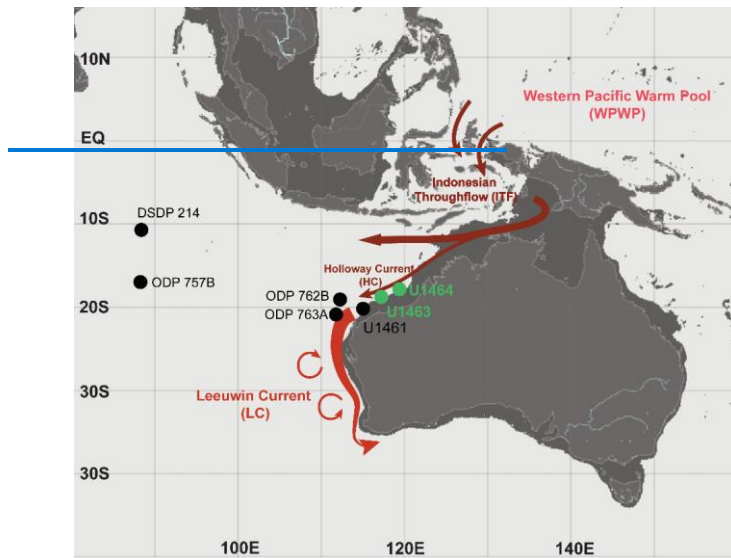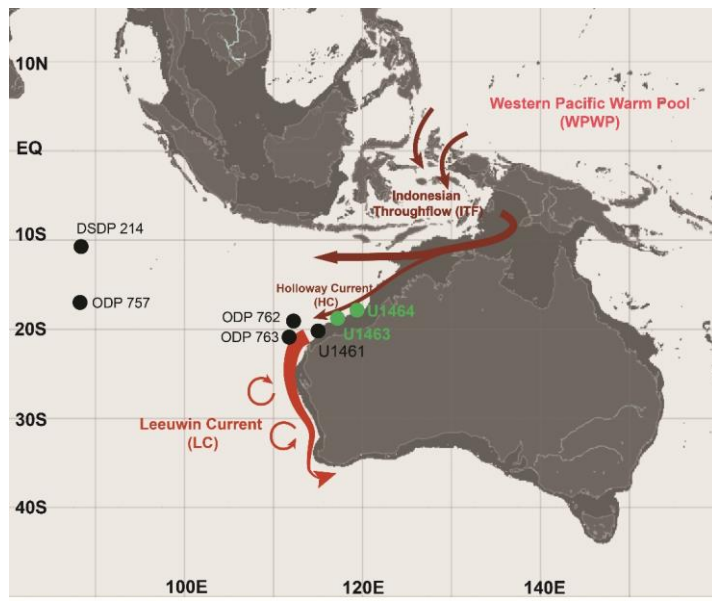
Figure 1: Modern bathymetric map indicating shelf~~al~~ environments (<200 m depth; dark grey shading) and site locations. IODP Sites U1463 and U1464 (NW Australian shelf; ~~NW Australian shelf; this study) are shown with~~ green dots) are the primary sites of investigation in this study~~circles~~. Other sites discussed in the text (black dots) include IODP Site U1461 (NW Australian shelf), ODP Sites 76~~3~~2 and ~~ODP~~ 76~~2~~3 (Eastern Indian Ocean), as well as ODP Site 757~~B~~ and DSDP Site 214 (equatorial Indian Ocean)~~, are discussed in the text and shown in black dots~~circles. The main surface oceanography of the Indo-Pacific region, including the ITF (dark red ~~lines~~arrows) and main path of the LC (lighter red ~~line~~arrow; adapted ~~by~~from (~~Auer et al., 2019; Gallagher et al., 2009) and the HC, which in this study are considered as one, are shown. ~~Also shown, the main surface oceanography of the Indo-Pacific region (dark red lines) and main path of the LC (lighter red line; adapted by (Auer et al., 2019; Gallagher et al., 2009) and the HC, which in this study are considered as one.~~ The ~~b~~Base map was generated using the ocean data visualization tools of E.U. Copernicus Marine Service Information (MYOCEAN PRO).

Information on the existence and strength of the LC in the latest Miocene and Pliocene remains limited, although a possibly active LC has been inferred from upper water column temperature and primary productivity reconstructions at its source area (IODP Expedition 356 Site U1461; Figure 1) for the interval spanning from 6-4 Ma (He et al., 2021). During that time, increased river runoff and humid conditions were prevailing in the area, under an intensified Indonesian Throughflow (ITF) (Auer et al., 2019; Christensen et al., 2017; He et al., 2021; Karatsolis et al., 2020). Previous investigations have demonstrated that ~~the~~ nannofossil assemblages can ~~has the potential to~~ reflect ~~ocean circulation changes in the area and closely track the~~ ITF source water variations and LC activity during the late Pliocene to Pleistocene (Auer et al., 2019), as well as record ~~. At the same time, evidence for~~ broader changes in ~~the~~ the ocean's nutrient budget. Evidence for the latter ~~one~~ comes from the significant decrease in fluxes of the opportunistic, fast-growing (bloom-forming) species ~~of~~ within the assemblages, ~~which~~

significantly decreased their fluxes from 4.6–4.4 Ma, which markedrecording the end of the late Miocene to early Pliocene biogenic bloom in warm over the NW Australian shelf (Karatsolis et al., 2020;, 2022).

In this study, we aim to further constrain the latest Miocene to early Pliocene ITF and LC history, by identifying the key changes in the calcareous nannofossil assemblages. To achieve that, we extend the nannofossil record database from IODP Site U1463 (Auer et al., 2019; 3.65-2.97 Ma) back to ~5.7 Ma and present one more astronomically-tuned record from IODP Site U1464, that is located ~100 km away but in a different basin, dating back to ~6 Ma (Gallagher et al., 2017a;, Karatsolis et al, 2020). We evaluate the use of a ratio between three abundant taxonomic groups (genera) as an index to trace long-term shifts in water-column stratification and regional ocean circulation. Comparison with newly constrained temperature gradients between the NW Australian shelf and the eastern Indian Ocean further assists in identifying the possible underlying mechanisms for the observed changes. Finally, nannofossil evidence is put in a broader perspective in an effort to differentiate between signals that reflect basin-wide or global changes in nannoplankton evolution and the ocean's nutrient budget, and those that occurred due to regional ocean circulation and intensity of seasonal variations. Such decoupling of regional signals from overlying global patterns is crucial when using the nannofossil assemblages to reconstruct the evolution of the LC, as well as other boundary currents and ocean circulation patterns in dynamic shelfal environments.
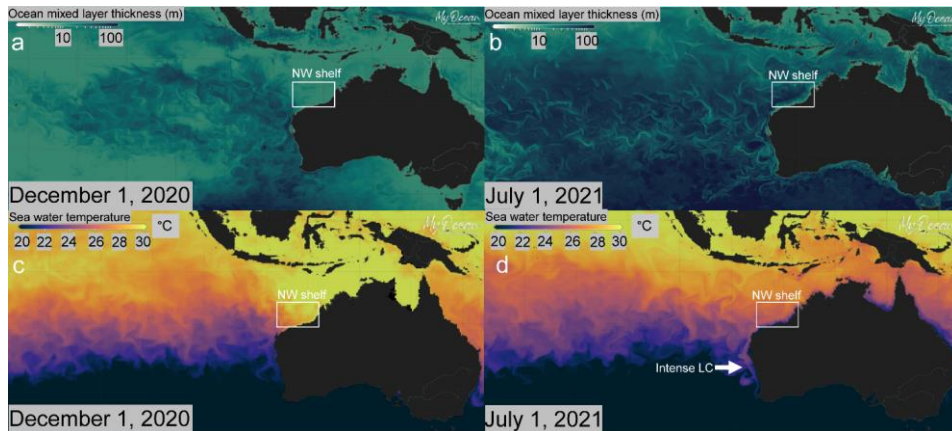
Figure 2: Present-day ocean circulation maps of the southeastern Indian Ocean area for the 1st of December 2020 (austral summer; **a-, c)** and 1st of July 2021 (austral winter; **b-, d)**. LC is weak during austral summer causing **(a)** reduced depth of the (a) mixed layer and increased stratification (a) and **(c)** higher SST (c) in over the NW Australian shelf. The LC intensifies during austral winter, while when **(b)** water column mixing in the eastern Indian Ocean increases and **(d)** SST decreases in the NW Australian shelf area (b, d); at the same time, it transports warmer surface waters further to the south (d). The sea surface cooling effect observed in shelfal environments during July is less pronounced further offshore. Maps were generated using the ocean data visualization tools of E.U. Copernicus Marine Service Information (MYOCEAN PRO) and dataset layer GLOBAL_ANALYSIS_FORECAST_PHY_001_024 (https://doi.org/10.48670/moi-00016) and GLOBAL_ANALYSIS_FORECAST_BIO_001_028 (https://doi.org/10.48670/moi-00015).
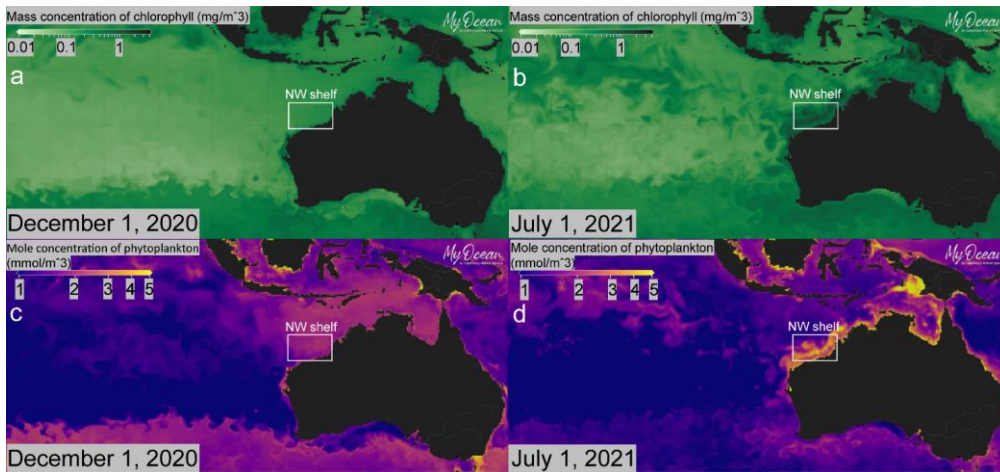
Figure 3: Present-day ocean productivity maps of the southeastern Indian Ocean area for the 1st of December of 2020 (austral summer; **a**, **c**) and 1st of July of 2021 (austral winter; **b**, **d**). Reduced LC and increased water column stratification during austral summer leads to low concentrations of **(a)** chlorophyll and **(c)** phytoplankton in the NW Australian shelf area. Intense LC and storm track activity during austral winter leads to increased water column mixing in the NW Australian shelf and significantly higher **(b)** chlorophyll and **(d)** phytoplankton concentrations. Maps were generated using the ocean data visualization tools of E.U. Copernicus Marine Service Information (MYOCEAN PRO) and dataset layer GLOBAL_ANALYSIS_FORECAST_BIO_001_028 (https://doi.org/10.48670/moi-00015).

2 Material and Methods

2.1 Nannofossil Counts

IODP Expedition 356 Sites U1463 (145 m water depth; 18°59′S, 117°37′E) and U1464 (270 m water depth; 18°03.9115′S, 118°37.8935′E) (Figure 1) yielded a stratigraphic succession from the late Miocene to the early Pleistocene, with abundant, moderately preserved calcareous nannofossils. Note that the late Miocene to Pliocene sediments were deposited at much greater depths than the current water depth suggests, mirroring at the time of deposition middle/outer shelf to upper bathyal conditions (Christensen et al., 2017; Gallagher et al., 2017). Core sample ages are based on the tuned age models for Site U1463 (Groeneveld et al., 2021) and Site U1464 (Karatsolis et al., 2020).

A total of 209 samples (104 samples from Site U1463 and 105 samples from Site U1464) were prepared for micropaleontological analysis, with a sampling interval of ~1.5m (at least one sample per core section). Sample preparation followed the 'drop technique' (Bordiga et al., 2015). For each sample, 5 mg of dried bulk sediment was weighed and initially diluted with 20 mL of ammonia-buffered water. After short sonification (30-60 seconds), the suspension was passed through

a 63 µm-meshed sieve and further diluted to three different final concentrations (bulk-weight equivalent concentrations of ~0,125 mg/mL; 0,08 mg/mL; 0,04 mg/mL). Subsequently, 1.5 mL of well-mixed suspension was placed on a cover slip with a high-precision micropipette, and the sample was dried on a hotplate at 60°C. Finally, cover slips were mounted on glass slides with Norland Optical Adhesive (NOA61) and cured under a UV light source for approximately half an hour.

Micropaleontological analysis was conducted using polarized light microscopy at 1000 × magnification, with at least 300 specimens counted and identified at genus level per sample. ~~Coccoliths~~Nannofossils ~~within~~ of the *Reticulofenestra* and *Gephyrocapsa* genera were further classified by size categories of <3µm (small), 3-5µm (medium) and >5µm (large). Samples from different ~~initial~~ dilution concentrations were selected, based on the abundance of nannofossils ~~in the samples~~on the slides. Confidence intervals for nannofossil relative abundance were calculated using the binomial error function (95% CIs) in PAST 4 freeware (Hammer et al., 2001), as suggested by Suchéras-Marx and others (2019). Subsequently, absolute abundances (in nannofossils per gram of sediment, (N/g)) of the different genera and morphospecies were calculated using the following equation (e.g., Koch and Young, 2007):

$$(1)\ \text{Abs. Abundance (AA)} = \frac{N \times A}{f \times n \times W}\ ,$$

where A is the area of the cover slip (mm²), N is the total number of nannofossils counted, f is the area of one field of view (FOV; mm²), n is the number of FOV, and W is the equivalent dry bulk sediment weight on the cover slip (g). Reproducibility for the absolute abundance calculation is estimated to be ±10-15% (Bordiga et al., 2015).

Nannofossil fluxes were calculated following the formula:

$$(2)\ \text{NAR} = \text{AA} \times \text{LSR} \times \text{DBD}\ ,$$

where NAR stands for nannofossil accumulation rates (N/cm² kyr), AA is the absolute abundance of ~~coccoliths~~nannofossils (in N/g), LSR is the linear sedimentation rate (in cm/kyr) calculated between astronomically-tuned tie points and DBD is the average dry bulk density (in g/cm³), calculated for the studied interval from available data ~~found~~ in the IODP LIMS ~~database~~online report portal (https://web.iodp.tamu.edu/LORE/) ~~dry bulk density of the sample (in g/cm³)~~. Nannofossil flux records older than 5.8 Ma at ~~IODP~~ Site U1464 were not included in the interpretation of changes in nannofossil abundances~~Nannofossil flux records older than 5.8 Ma at IODP Site U1464 were not considered~~, ~~since~~because they are ~~potentially linked to driven~~biased by the very high sedimentation rates ~~that were observed~~ following the abrupt, late Miocene deepening of the Roebuck basin (Karatsolis et al., 2020). ~~Despite that~~Nevertheless, relative nannofossil abundances~~,~~ ~~were~~can ~~still be considered to~~that reflect changes in the assemblage~~s, and are therefore presented,~~ extending the record at ~~IODP~~ Site U1464 back to ~6 Ma. ~~All nannofossil data were placed on the tuned age models for U1463 and U1464, as presented by Groeneveld and others (2021) and Karatsolis and others (2020).~~

2.2 Correspondence analysis (CA) and Shannon ~~d~~Diversity ~~i~~Index (H)

Correspondence analysis (CA) and calculation of the Shannon ~~d~~Diversity ~~i~~ndex (H) (Shannon, 1948) were conducted using PAST 4 freeware (Hammer et al., 2001). We applied CA to the nannofossil time series data, in order to compare samples of

170 different age based on the relative abundance of species present in each sample (column principal with ages representing distinct columns). This allowed for identification and visualization of possible breaking points where species composition and the structure of the assemblage significantly changed through time. However, this ordination method does not provide measures of statistical significance, and therefore only serves to confirm, by observations in multivariate space, the main trends observed in the raw data. CA was chosen over cCanonical cCorrespondence aAnalysis (CCA), because our time series do not

175 include any additional environmental parameters (no environmental gradient extraction). The H index was calculated to spot shifts in nannofossil diversity and identify intervals of species overturn. The H index varies from 0 for assemblages consisting of a single species to high(er) values for assemblages with many species, but each represented by few individuals.

2.3 Nannofossil sStratification iIndex

180 A ratio between the three most common genera of the assemblage, namely bloom-forming *Reticulofenestra* and *Gephyrocapsa* species and *Sphenolithus* spp., was calculated to investigate relative changes in water column conditions and was named nNannofossil sStratification index (NSI). Species comprising this ratio are abundant throughout the record until the extinction of *Sphenolithus* spp. at ~3.54 Ma (Gradstein et al., 2012), while no long-term decreasing trend in the relative abundance of *Sphenolithus* was observed in the time preceding its last occurrence (LO; Figures A1, A32). The calculation followed the

185 equationratio was calculated as follows:

$$(3)\ \text{NSI} = \frac{\text{Sph}}{\text{Sph}+(\text{Rm}+\text{Rs}+\text{Gs})}\ ,$$

where Sph, Rm, Rs and Gs represent the relative abundances of *Sphenolithus* spp., medium-sized *Reticulofenestra* and small-sized *Reticulofenestra* and *Gephyrocapsa* species, respectively.

190 Of the nannofossil groups comprising this ratio, small sized *Reticulofenestra* species have been demonstrated to thrive in unstable conditions during the Pliocene, since they were favoured by more pronounced seasonality and tidal mixing (Auer et al., 2019; Ballegeer et al., 2012). With a similar ecological affinity, medium-sized *Reticulofenestra* species reflected neritic conditions with increased nutrient availability through local upwelling activity (Auer et al., 2019 and references therein). Small *Gephyrocapsa*, although also considered bloom-forming, highly opportunistic species, were adapted to warmer and more

195 stratified water masses, as commonly inferred in subtropical continental margins (Auer et al., 2019; Boeckel and Baumann, 2008; Okada and Wells, 1997; Takahashi and Okada, 2000). *Sphenolithus* spp. on the other hand, although of complex paleoecological affinity that ranges from low-latitude, oligotrophic warm waters (e.g., Gibbs et al., 2004; Haq, 1980; Haq and Lohmann, 1976) to restricted mesotrophic ocean masses (Wade and Bown, 2006), has been commonly grouped with *Discoaster* as characteristic of warmer, more stratified water conditions compared in contrast to the bloom-forming

200 *Reticulofenestra* and *Gephyrocapsa* species (e.g. Gibbs et al., 2005; Haq and Lohmann, 1976). Similar ratios between "cool", mesotrophic species and "warmer", oligotrophic species have been used in the pastassessing the paleoecology for during other

geological periods. For example, the ratio between species of the genus *Toweius* with *Sphenolithus* and *Discoaster* has been used as a paleoenvironmental index for the Paleocene-Eocene thermal maximum (Gibbs et al., 2010). Species of the genus *Toweius* have been characterised as meso/eutrophic, having occupied a ~~similar~~ niche similar to the modern bloom-forming species (e.g. Bralower, 2002; Gibbs et al., 2010). ~~Similarly, a ratio between *Reticulofenestra* species and *Florisphaera* has been used to monitor changes in the nutricline and thermocline during the Pleistocene (Flores et al., 2000).~~ We therefore propose that the ~~ratio~~ NSI ~~of *Sphenolithus* spp. to bloom-forming species~~ can serve as a useful indication of changes in water column mixing and nutrient availability and has the potential to record relative stratification above the NW Australian shelf during the latest Miocene to Pliocene. ~~For this reason, we will be referring to this ratio as the nannofossil stratification index (NSI).~~

2.4 Shelf-to-offshore pPaleotemperature ~~proxies and~~ gradient~~s calculation~~

Paleotemperature gradients between ~~three~~ sites located in the eastern Indian Ocean (DSDP Site 214 and~~,~~ ODP Site 763A~~)~~ and the NW Australian shelf (IODP Site U1461) (Figure 1), were calculated based on available proxy-based estimates. At ~~IODP~~ Site U1461, two paleotemperature proxy records include archaeal membrane lipids ('GDGTs') ~~glycerol dialkyl glycerol tetraethers (GDGT)~~-based TEX$_{86}$ and alkenone-based U$^{k'}_{37}$ temperatures (He et al., 2021), spanning the interval from ~6-3.5 Ma. At ~~ODP~~ Site 763A and ~~DSDP~~ Site 214, available records consist of Mg/~~Ca~~ Ca-derived temperatures from *Trilobatus sacculifer* foraminifera (Karas et al., 2009, 2011). A direct site-to-site comparison based on the same paleotemperature proxies is therefore not possible. However, the quality and temporal resolution of each record are sufficient for the purpose of contrasting overall and long-term shelf-to-offshore temperature trends, despite potential biases between proxies. ~~These proxies record temperature from different depths~~Alkenone-producing~~,~~ ~~with U$^{k'}_{37}$ reflecting the alkenone producing~~ haptophytes ~~that live in the photic zone and therefore SST~~ (e.g. Eglington et al., 2001; Müller et al., 1998) and ~~Mg/Ca the~~ of the water column, ~~where~~ *Trilobatus sacculifer* calcifies in the upper 50 m of the water column in the tropics (e.g., Anand et al., 2003; Dekens et al., 2002), therefore the U$^{k'}_{37}$ and Mg/Ca proxies reliably reflect sea surface temperature (SST). On the other hand, TEX$_{86}$ estimates appear to be more complicated and although ~~they are~~ widely used to reconstruct SSTs, they ~~can in cases~~may in some cases record temperatures ~~up~~down to >200 m depth (van der Weijst et al., 2022). This is mainly attributed to the fact that GDGTs are produced by Thaumarchaeota throughout the water column and therefore deeper-water species also contribute to the sedimentary composition of this proxy (Kim et al., 2016). ~~Indicative of that is the fact that a~~Along the Australian shelf, Pliocene and ~~-~~Pleistocene records of TEX$_{86}$ have been used both as SST indicators (e.g., De Vleeschouwer et al., 2019; Smith et al., 2020), or containing a deeper signal (Smith et al., 2013), with the record from Site U461 assumed to ~~used in this study~~ reflect~~ing~~ an integrated 0-200m water column depth (He et al., 2021). However, during the early Pliocene, only a ~~low~~small vertical thermal difference ~~has been~~was inferred ~~for~~at this site, based on the difference between the "shallower" U$^{k'}_{37}$ and the "integrated 0-200m" TEX$_{86}$ temperature signals (He et al., 2021)~~, indicating that these two proxies might have been recording~~

a similar depth at that time. DueBecause of to this factobservation, andas well as the lack of Mg/Ca records from the shelf and no, as well as a $U_{37}^{k'}$ recorddata older than 5.5 Ma on the shelf, we decided to included TEX$_{86}$ in the comparisons, despite the potential differences in depth estimates. Four pairs of temperature gradients were calculated between samples with the closest assigned age, as well as. medians of the differences between assigned ages.. The gradients between $U_{37}^{k'}$ proxy estimates and Mg/Ca-based estimates were labelled as "ΔSST" (ΔSST$_{U1461-763}$, ΔSST$_{U1461-214}$), whereas the onesthose between TEX$_{86}$ TEX$_{86}$ and Mg/Ca as "ΔT" (ΔT$_{U1461-763}$, ΔT$_{U1461-214}$), to account for a potential bias from a subsurface signal in the TEX$_{86}$ proxy and track related discrepancies. The median of the age difference between sample pairs was calculated as an error in our considerations of long-term trends.

3 Results

3.1 Nannofossil relative abundances and fluxes

Calcareous nannofossils are very abundant and moderately preserved throughout the studied interval. Preservation was initially assessed to be moderate to good (scores 2 and 3, Gallagher et al., 2017b, Gallagher et al., 2017c), but a re-assessment through visual inspection showed that good preservation was actually rare. Coccolith NAR and relative abundances reveal highly similar patterns at both sites, with bloom-forming *Reticulofenestra* (<5μm) and *Gephyrocapsa* (<3μm) species always dominating the assemblage (combined ~60-97%; Figures A1, A2; Figures A1, A3). The smallest bloom-forming species (<3μm *Reticulofenestra* and *Gephyrocapsa* species) were common to abundant throughout, ranging from ~30-97%. The next most common species was medium-sized *Reticulofenestra* (3-5μm), which constituted ~2-47% of the assemblage at Site U1463 and ~6-52% at Site U1464. *Sphenolithus* spp. reached up to ~20% at Site U1463 and ~23% at Site U1464, until it dramatically decreased at ~3.54 Ma, following the global pattern of extinction of the genus (Figures A1, A2). Other commonly occurring species were *Calcidiscus* spp., that constituted up to ~7% at both sites, *Umbilicosphaera* spp., with relative abundances up to ~10% at Site U1463 and ~9% at Site U1464 and larger (>5μm) *Reticulofenestra* species, with percentages up to ~11% at Site U1463 (Figure A3) and ~9% at Site U1464 (Figure A4). Consistently present species, but with very low relative abundances, were *Helicosphaera* spp. and *Discoaster* spp. Total NAR ranged from ~2× 10^{10} to ~3× 10^{11} N/cm^2 kyr at Site U1463 and ~2× 10^{10} to ~2× 10^{11} N/cm^2 kyr at Site U1464 (not shown).

Two time intervals can be identified that represent distinct changes in nannofossil assemblage composition and NAR of the most common species (Figures A1, A2). The first one occurred from 5.4–5.2 Ma and was characterized by a ~10% increase in relative abundance (and NAR) of bloom-forming species and a synchronous ~10% decrease in relative abundance (and NAR) of *Sphenolithus* spp. at both sites. The fact that the burial fluxes (NAR) changed in opposite direction supports the assumption that these taxonomic groups have distinct ecologies and were both affected simultaneously (Figures A5, A6). At the same time, bulk sediment mass accumulation rates (MARs) do not demonstrate any notable, sustained change, indicating that the observed pattern in the assemblage composition was driven by changes in species' abundance (Figures A55, A672). *Umbilicosphaera*

spp. and large *Reticulofenestra* species had a distinctive low in relative abundances during this period, whereas *Calcidiscus* spp. was not significantly influenced (Figures A3, A4).

The second interval occurred from 4.6–4.4 and represents a rapid decrease in total NAR, mainly driven by the decrease in abundance of small *Reticulofenestra* species (Karatsolis et al., 2020), as well as a basin-wide decrease in low-latitude paleoproductivity (PP; Karatsolis et al., 2022). During this interval, the relative abundances of other common species such as *Calcidiscus* spp. and *Umbilicosphaera* spp. increased and remained steadily higher compared to the interval before 4.6 Ma (Figures A23, A4), while their fluxes were not significantly affected (Figures A76, A8).demonstrated increased NAR and a stepwise increase in relative abundance (Figures A1 and A2). Large *Reticulofenestra* species virtually disappeared during this interval (Figures A7, A8), following the rapid decrease in NAR of the smaller species of their the same genus (Figures A5, A6A6, A82). As NARs of small *Reticulofenestra* spp. decreased, the small *Gephyrocapsa* spp. species started to increase (~4.45–4.42 Ma) in percentage. Small *Gephyrocapsa* spp. and became dominant from ~4.2 Ma until the end of the studied interval, with maximum NAR values of ~1 × 10^{11} N/cm^2 kyr at IODP Site U1463 and ~5 × 10^{10} N/ cm^2 kyr at IODP Site U1464, which corresponds to ~70% and ~60% of the total assemblage respectively. After ~4.4 Ma, the NAR of *Sphenolithus* spp. bounced backreturned to higher values, especially at IODP Site U1463, presenting showing distinct peaks that are centred at ~4.1 Ma and 3.7 Ma. This species'Its relative abundance increased too, occasionally reaching in cases values of >10%, although it never reached its maxima as during the latest Miocene maxima (Figures A1, A32).

3.2 Nannofossil multivariate analysisstratification index (NSI)

285

Changes in NSI covary throughout the studied interval and correlate well between the two sites (Figure 4a).As is the case for the nannofossil assemblage compositions, changes in NSI correlate well between the two sites and covary throughout the studied interval (Figure 4). A stepwise decrease is observed from 5.4–5.2 Ma, which mirrors the overall decrease in relative abundance and NAR of *Sphenolithus* spp. and the synchronous increase in small *Reticulofenestra* species. After ~4.2 Ma, NSI
290 shows higher variation with short intervals of higher values (4.2-4 Ma and 3.8-3.54 Ma). These intervals correspond to peaks in relative abundance of *Sphenolithus* spp.After ~4.2 Ma, this surface water stratification proxy shows higher variation with small intervals of higher values (4.2-4 Ma and 3.8-3.54 Ma), that correspond to peaks in relative abundance of *Sphenolithus* spp. Between 4 and 3.8 Ma, NSI showsdemonstrates low values, whereas after 3.54 Ma, the last occurrence (LO) of *Sphenolithus* spp. makes the index non-applicable. The H-index (Figure 4b) demonstrates that the most distinct change, which
295 collectively influenced the nannofossil species distribution, occurred from 4.6–4.4 Ma and was marked by a stepwise increase in diversity. Notably, no sustained change in diversity is observed during the interval of stepwise decrease in NSI (5.4–5.2 Ma; Figure 4a).

300
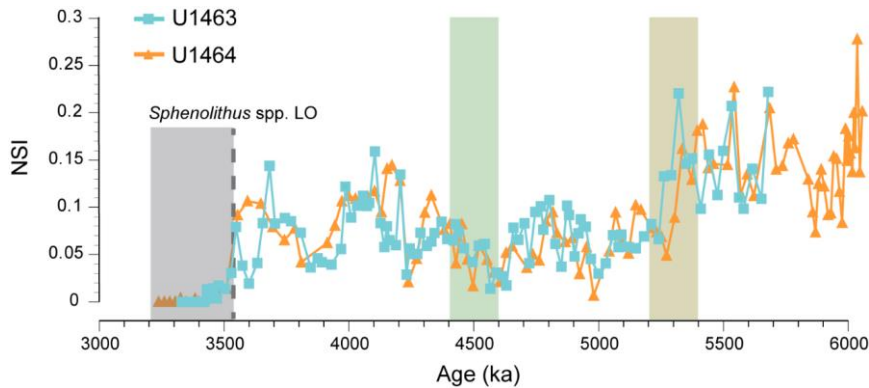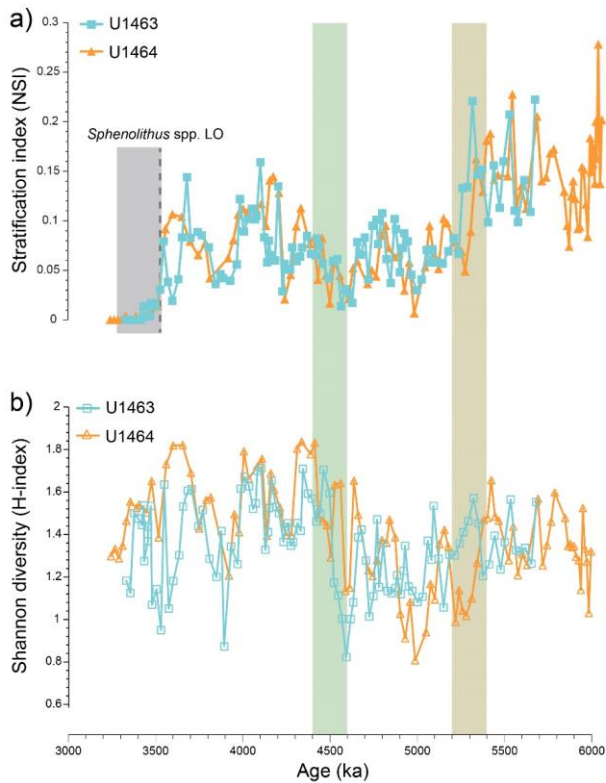
Figure 4: (~~Latest~~ a)~~,~~ Miocene to early Pliocene nannofossil stratification index (NSI) at IODP Sites U1463 (~~light~~ blue squares) and U1464 (orange triangles). ~~Brown shaded area represents the stepwise decrease in NSI and increase in NAR of bloom-forming species. Green shaded area represents the interval of significant decrease in PP and NAR of bloom-forming species.~~ Dashed grey line indicates the ~~l~~Last
305 ~~o~~Occurrence (LO) of *Sphenolithus* spp. during the early Pliocene (~3.54 Ma). Therefore, this NSI cannot be used for younger samples (grey shading). (**b**)~~,~~ Shannon ~~d~~Diversity (H-index) ~~calculated using PAST 4 software and plotted against sample age (ka)~~ at ~~IODP Sites U1463 (light blue squares) and U1464 (orange triangles)~~the same sites. Brown shad~~ed~~ing~~area represents~~highlights the stepwise decrease in NSI and increase in NAR of bloom-forming species. Green shad~~ed area~~ing represents the interval of significant decreases in paleoproductivity (PP) and NAR of bloom-forming species.

310

~~3.3 Correspondence Analysis (CA) and Shannon Diversity Index (H)~~

By color-coding the samples based on their age across the main time intervals of interest (5.4-5.2 Ma and after 4.6–4.4 Ma; Figure 5), we test if any of the observed changes in the abundance of dominant species were accompanied by ~~larger~~ shifts in

315 the relationship between relative abundances of species in multivariate space. ~~By color-coding the samples based on their age and major changes in the assemblage, namely distinct time intervals identified before 5.4 5.2 Ma and after 4.6 4.4 Ma (Figure 5), we test if any of the changes led to shifts in the relationship between relative abundances of species in multivariate space and therefore to significant restructuring of species compositions.~~ Correspondence analysis at both sites mainly highlights the changes that occurred during 4.6–4.4 Ma, almost splitting the samples that belong to the period before the rapid decrease in

320 NAR from those after that across the primary CA axis (Figure 5a, b). It also ~~separates and links~~groups the species that were more dominant before and after ~4.4 Ma with the respective interval of dominance (low angle from the (0,0) source between species and sample age). ~~The separation occurs between s~~Species such as small *Reticulofenestra* and *Sphenolithus* spp. are separated from small *Gephyrocapsa*, *Calcidiscus* spp. and *Umbilicosphaera* spp. (Figure 5). Medium-sized *Reticulofenestra* appears to have a less clear affinity, being close to the primary axis and on opposite sides of it at ~~IODP~~ Sites U1463 and U1464.

325 This can probably be attributed to the fact that this species showed relatively stable relative abundances and two distinct peaks before and after the 4.6–4.4 Ma event (Figure A9~~B1~~), which could also explain the few before/after 4.4 Ma samples that fall on the same side of the axis (Figure 5a, b). Interestingly, species loadings and <4.4 Ma sample scores correlate well, and both appear to be situated further from the (0,0) source, demonstrating that the association of common species with the younger part of the record is stronger. ~~Finally, the H index also demonstrates that the most distinct change, which collectively influenced~~

330 ~~the nannofossil species distribution, occurred from 4.6 4.4 Ma and was marked by a stepwise increase in diversity (Figure 4b6). Notably, no sustained change in diversity is observed during the interval of stepwise decrease in NSI (5.4 5.2 Ma; Figure 4a).~~

a U1463 Correspondence Analysis (CA)

1 small *Reticulofenestra*
2 *Reticulofenestra* spp. 3-5 μm
3 *Sphenolithus* spp.
4 small *Gephyrocapsa*
5 *Pseudoemiliania lacunosa*
6 *Calcidiscus* spp.
7 *Umbilicosphaera* spp.
8 *Helicosphaera* spp.

+ >5.25 Ma
○ 4.4-5.25 Ma
□ <4.4 Ma

b U1464 Correspondence Analysis (CA)
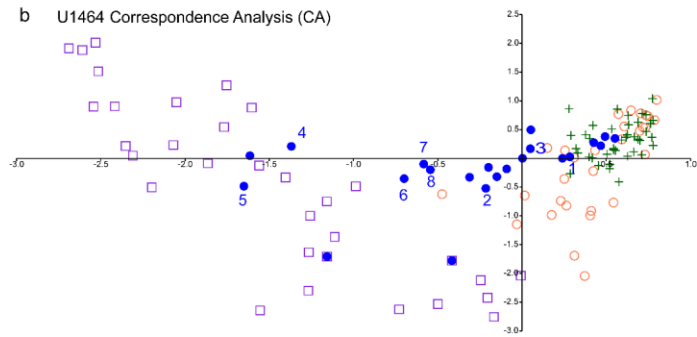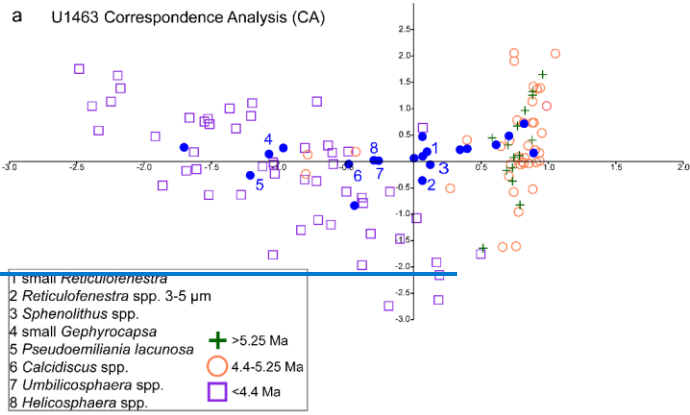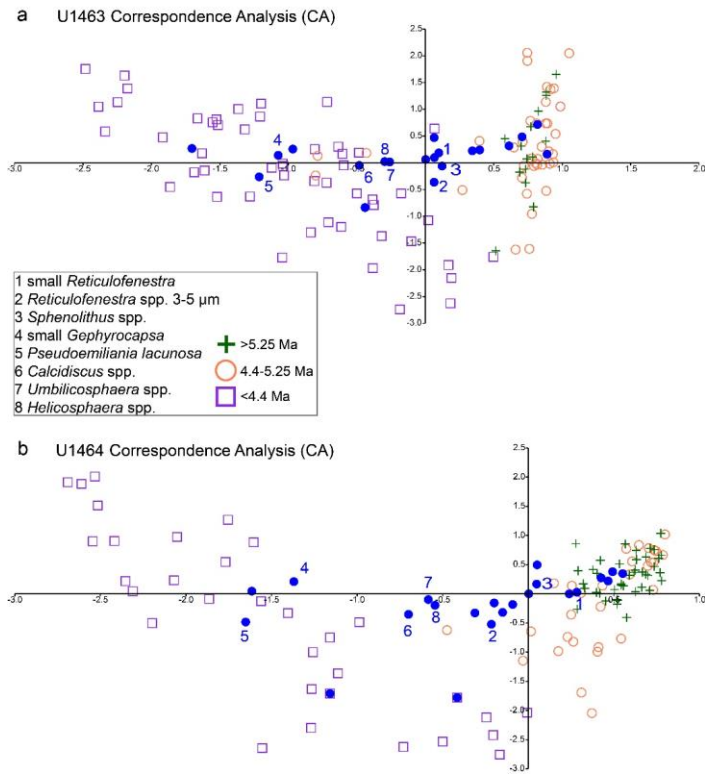
335

Figure 5: Correspondence aAnalysis (CA) for IODP Sites U1463 (**a**) and U1464 (**b**). Orange circles represent samples older than s prior to 5.25 Ma and together with the green crosses plus signs (4.4-5.25 Ma) constitute the records prior to the significant decrease in NAR that occurred at 4.6 4.4 Ma. Purple Boxes squares in purple represent sample ages <4.4 Ma. Numbered (1-8) blue points dots represent the most common nannofossil species (see legend).

 Formatted: Font: Not Bold
Formatted: Font: Not Bold
Formatted: Font: Not Bold
Formatted: Font: Not Bold
Formatted: Font: Not Bold
Formatted: Font: Not Bold
Formatted: Font: Not Bold
Formatted: Font: Not Bold
Formatted: Font: Not Bold
Formatted: Font: Not Bold
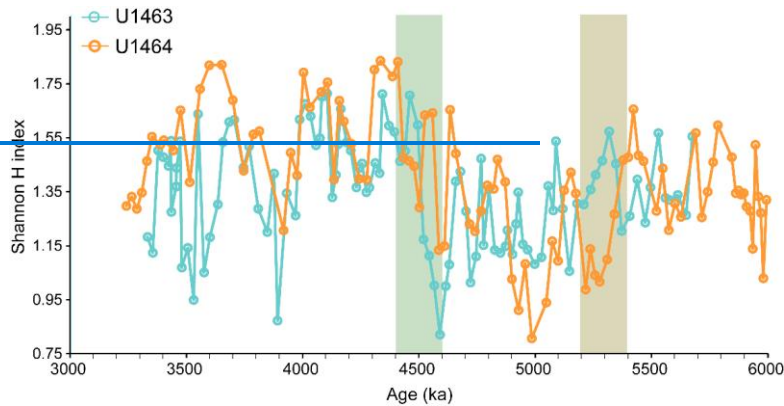
Figure 6: Shannon Diversity Index (H) calculated using PAST 4 software and plotted against sample age (ka) at IODP Sites U1463 (blue) and U1464 (orange). Brown shaded area represents the stepwise decrease in NSI and increase in NAR of bloom-forming species. Green shaded area represents the interval of significant decrease in PP and NAR of bloom-forming species.

345 **3.3 Paleotemperature gradients**

The median difference between closest sample ages for any pair of sites ranged between ~2-10 kyr (Table AD1), although in one case, due to a gap of >200 kyr in sample spacing at DSDP Site 214, the sample age difference became was ~100 kyr (~3.75-3.96 Ma) for gradients involving this site. However, this gap in paleotemperature estimates occursred towards the end of our studied interval and therefore does not limit our potential to investigatinge possible links to sustained changes in the
350 nannofossil assemblages that occurred across the Miocene-/Pliocene boundary and between 4.6–4.4 Ma. Despite the different previous interpretations of the temperature proxies, their gradientsAll records demonstrate highly similar comparable long-term patterns; they, and co-vary throughout the Pliocene and can be separated in three distinct intervals (Figure 6). The first one occurs bBefore ~5.2 Ma, when all gradients have positive values, demonstrating that temperatures at Site U1461 were consistently higher at this time than those in the eastern Indian Ocean. Being the However, oonly one gradient ($\Delta T_{U1461-763}$)
355 with is based on more than 3 samples, and $\Delta T_{U1461-763}$ is the most informative gradient for the interval >5.2 Ma and therefore for the latest Miocene. Between 6-5.2 Ma, this temperature gradient hads a median value of ~2 °C and decreased to, which then becomes -0.6 °C for the interval between 5.2-2.5 Ma, likely driven by a cooling at Site U1461 and a warming at Site 763A (Figure 67). This indicates that TEX$_{86}$ temperatures at Site U1461 transitioned from a phase of steadily warmer conditions to slightly cooler values compared to Site 763A. In general, $\Delta\Delta$SST values gradients are lower smaller than ΔT,
360 with median values of -0.2 and -0.5 °C for ($\Delta SST_{U1461-763}$, $\Delta SST_{U1461-214}$ 214) and versus -0.63 and -1.14 °C for ($\Delta T_{U1461-763}$, $\Delta T_{U1461-214}$) respectively for the interval from 5.2-3.5 Ma (see Table AD1). Median values also reveal that, both for the ΔSST and the ΔT records, gradients are generally higher greater between Site U1461 and DSDP Site 214 than those between Site U1461 and Site 763A. After 5.2 Ma and until ~4.3 Ma, gradients have negative values (reflecting lower temperatures over the

shelf) and show small fluctuations between 0 and -2 °C, whereas after ~4.3 Ma fluctuations become more intense and vary significantly from ~ -3.5 to 2 °C. Despite this strong variation, positive gradient values never exceed the onesthose observed before 5.2 Ma and mostly remain mostly negative, indicating that warmer conditions were prevailing in the eastern Indian Ocean, whereas waters over the shelf were generally cooler.
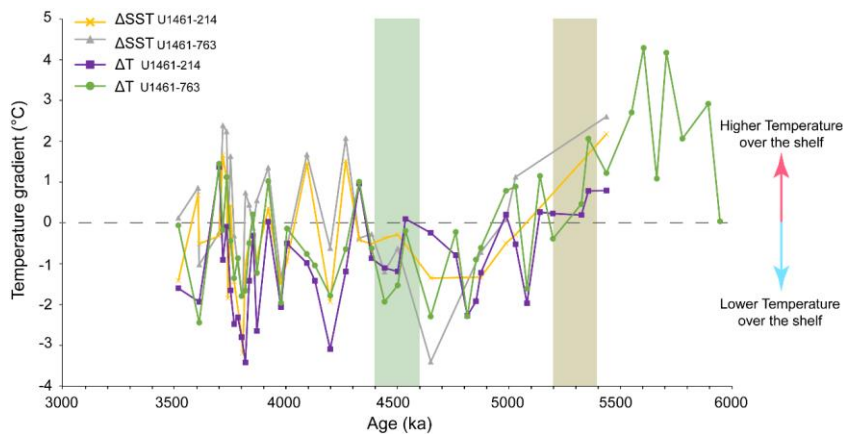
Figure 67: Temperature gradients (ΔT and ΔSST and ΔT) between IODP Site U1461 (NW Australian shelf), ODP Site 763A (Exmouth Plateau) and DSDP Site 214 (eastern Indian Ocean). Gradients are calculated between the TEX₈₆ and Mg/Ca records (ΔT) and between $U^{k'}_{37}$ and Mg/Ca records (ΔSST) and the TEX₈₆ and Mg/Ca records (ΔT) for the interval 6-3.5 Ma. Horizontal grey dashed line indicates no difference in temperature (ΔT, ΔSST, ΔT = 0°C). Brown shaded area-ing represents corresponds to the stepwise decrease in NSI and increase in NAR of bloom-forming species. Green shadinged area represents the interval of significant decrease in PP and NAR of bloom-forming species.

4 Discussion

4.1 Water column mixing and nutrient availability on the NW Australian shelf

The common species comprising the NSI, namely small bloom-forming species and *Sphenolithus* spp., provided the bulk of the nannoplankton biomass and productivity and can therefore be expected to represent species that had broad ecological tolerances and the potential to record climate-biota interactions and feedbacks over long time intervals (e.g., Hannisdal et al., 2012; Henderiks et al., 2020). Additionally, sBecauseince the nannofossil abundance in each sample represents an average, smoothed record over thousands of years, it would be impossible to directly infer changes in seasonal and interannual variation of the ITF and LC in a similar way that modern plankton observations and climate models do. Despite thatNevertheless, it can be expected that changes in ocean circulation or seasonality that significantly influenced the flow path of major boundary currents over the course of thousands of years, would be mirrored in the mean nannofossil assemblage, favouring taxa that benefited seasonally or interannually by the prevailing conditions. Therefore, the NSI can give usoffers an indication of

persistent overall changes in water column stratification and mixing, that could be driven by a long-term switch in seasonal dynamics, ITF flow or LC intensity during the latest Miocene to Pliocene.

On this basis, the NSI reveals a stepwise phase of reduction in stratification and intensified nutrient replenishment in the upper water column, that took place around the Miocene-Pliocene boundary (5.4-5.2 Ma; Figure 4a). This suggests significant
390 environmental changes during that time and a transition from a more tropical stratified environment to a modern-like dynamic shelf~~al~~ area, favouring bloom-forming species over *Sphenolithus* spp. After its reduction, NSI never returned to its late Miocene levels, demonstrating that increased water column mixing was a prevailing regime in the area from 5.2-3.54 Ma, although an interval of overall higher NSI, with stronger amplitude~~some~~ variations between ~~and interchanging~~ higher and lower phases can be observed from ~4.2 to 3.54 Ma (Figure 4a). This indicates that intervals of relatively stronger stratification occurred
395 between 4.2-4.0 Ma and 3.8-3.54 Ma (higher NSI phases), while water column mixing was more intense between 4-3.8 Ma. Three possible mechanisms related to regional paleoclimate and ~~the~~ LC dynamics ~~in the area~~ could explain the observed pattern. The first ~~one~~ would suggest a strong effect of changes in upper water column stratification on primary productivity due to a LC acceleration, as it has been previously documented in a series of modern observational data and Pleistocene paleoclimatic records. Specifically, intensified LC activity has been linked to increased eddy formation that promotes ~~enhanced~~
400 productivity across the western Australian continental shelf (Auer et al., 2021; Feng et al., 2009; Furnas, 2007; Koslow et al., 2008; Thompson et al., 2011). This mechanism has also been proposed for other coastal areas influenced by boundary currents such as the southwestern Australian shelf (Harris et al., 1987; Koslow et al., 2008) and the Japanese coast (Kimura et al., 2000). Additionally, the modern observational and simulated data also show that the NW Australian shelf demonstrates increased water column mixing and phytoplankton productivity close to the shelf during austral winter when LC is stronger
405 (Figures 2 and 3). Since the presence of the LC depends on steeper steric height gradients between the source areas and the southern latitudes, we hypothesize that such steepening intensified during the early Pliocene, triggering enhanced seasonal flow of this major boundary current. In turn, intensified eddy activity and vertical mixing during the winter season and a subsequent "pumping" of nutrients from the continental slope onto the outer continental shelf, generated the observed long-term patterns in NSI, as well as the increase in NAR of bloom-forming species (Figures A5, A7~~6~~~~2~~).
410 A second mechanism that could explain the NSI decrease, is the overall increase in convective mixing across the continental shelf area ~~,~~due to ~~This could be the effect of~~ intensified cooling in the upper water column, as well as intensified storm activity during the winter period. ~~.~~ ~~These processes~~ ~~which~~ are known to have the potential for generating blooms by mixing the water column and bringing nutrients to the euphotic zone (e.g Chen et al., 2020; Longhurst, 2001). This mechanism was proposed for modern winter blooms along the west coast of Australia, which have been attributed to mixing of the upper water column
415 and a shoaling of the nutricline and chlorophyll maximum layer (Koslow et al., 2008).

The third mechanism comes in contrast to the first one and is based merely on the physical properties of the LC. According to that scenario, the warm SSTs and nutrient deficient waters that characterize the LC (Godfrey et al., 1986; Ridgway and Condie, 2004) should inhibit upwelling activity and stratify the water column, and therefore lead to overall decreased primary productivity, even across the continental shelf. Specifically, this relationship has been used to support the plausible LC activity

420 in the NW Australian shelf from 6-4 Ma, based on the low concentrations in the sediment of isoGDGTs and C28–C30 sterols (He et al., 2021). Similarly, a cooling during the Pleistocene along the NW Australian shelf has been previously attributed to a slowing down of the LC that would have allowed for intensified regional upwelling (Smith et al., 2020). Following the latter scenario, the reduction in NSI that we observe would be the result of a LC weakening, that allowed for seasonal upwelling and nutrient enrichment in the upper water column. However, it is worth noting that a similar cooling and intensification of

425 upwelling could be achieved by a long-term strengthening of the summer north-westerly winds that overcome the south-easterly trade winds and have the potential to generate seasonal upwelling. Since the above-mentioned scenarios are not mutually exclusive and involve processes that could have co-existed over long periods of time, a combination of mechanisms could explain the observed changes in NSI.

4.2 Paleotemperature and inferred ocean circulation patterns

430 Temperature gradients between the eastern Indian Ocean and the NW Australian shelf sites further support significant changes in ocean circulation during the late Miocene to Pliocene and compliment the observed changes in the nannofossil assemblages. In general, the higher ΔT gradient (in absolute values) after 5.2 Ma compared to the ΔSST, supports the hypothesis that TEX_{86} temperatures awere influenced by a slightly deeper and cooler signal of the integrated upper 200 m of the water column (He et al., 2021; Smith et al., 2013). Although these differences are consistent throughout the record, they are generally small and

435 therefore in good accordance with the low gradient between the integrated water column temperature and the SST ($\Delta T_{TEX86-U_{37}^k}$) for the interval between 6-3 Ma at IODP Site U1461 (median value of ~1.1°C; He et al., 2021). More importantly, the temperature differences derived from all proxies between the NW Australian shelf and the eastern Indian Ocean sites show similar variation and record a stepwise decrease of the temperature gradient between the two areas, driven by a cooling in the former area and a warming in the latter (Figure 78 a, b). The overall changeshift can be mainly tracked by the median values

440 of $\Delta T_{U1461-763}$ before and after 5.2 Ma, which suggest a shift of ~2.5°C that closes the temperature gap between the shelf and the eastern Indian Ocean, while flipping the temperature relationship between the two regions by making the latter one warmer. Similar temperatures across the NW Australian shelf and the eastern Indian Ocean indicate well-established ITF connectivity, in good agreement with the suggested warm and humid conditions that were prevailing in the area since the late Miocene (Christensen et al., 2017; Karatsolis et al., 2020; Stuut et al., 2020). Interestingly, this change also coincides with the decrease

445 in NSI from 5.4–5.2 Ma, suggesting a possible link between the changes in temperature and the stratification index (Figure 78 a, b), either by a decreased tolerance of *Sphenolithus* spp. to relatively cooler temperatures over the shelf, or through changes in nutrient availability due to intensified seasonal mixing and/or upwelling that favoured opportunistic species. On thea samesimilar note, both the NSI and the paleotemperature gradient records increase in amplitude between ~4.2-3.54 Ma, showing intervals of higher and lower values and peaks that are well correlated (both centred at ~4.1 and 3.7 Ma). That could

450 indicate a similar link of temperature and NSI inon shorter timescales, although such a correlation would need higher resolution paleotemperature and nannofossil records in order to be sufficiently established.

In principle,~~ ~~ a cooling at Site U1461 could be explained ~~either~~ by (i) cooler surface water that began to influence the area and decreased the average temperature, (ii) ~~or by~~ the weakening of the ITF and LC which would have allowed for seasonal upwelling of deeper, colder water to occur, or by (iii) a sustained increase in vertical mixing, that led to an overall decrease in temperature in the integrated upper water column. However, since evidence for significant restriction of the ITF or a switch of LC source are suggested to have occur~~red~~ much later, towards the late Pliocene (e.g. Christensen et al., 2017; Karas et al., 2011; De Vleeschouwer et al., 2019), ~~less stratification induced by intensified seasonality~~we suggest that an increase in water column mixing is the most probable scenario to have generated the observed changes in the average temperature signal. Furthermore, if ~~T~~this increase in mixing was driven by an overall intensification of seasonal extremes, it ~~c~~would have resulted in a deeper mixed layer and increased eddy formation along the Australian shelf ~~both due to~~because of both increased storm track ~~activity~~and LC activity ~~and related eddy formation during the winter season~~. ~~F~~Further evidence for the increased presence of the LC in the area comes from the temperature changes at ODP Site 763~~A~~. Records from this site have been previously used to infer the presence of this boundary current in the geological past (e.g., Auer et al., 2019; Karas et al., 2011) and it is located in an area that has been commonly used to test LC activity through Ocean General Circulation models (Godfrey, 1996; Hirst and Godfrey, 1993). At ~~ODP~~ Site 763~~A~~, we observe a distinct increase in SST of ~2°C (Figure 7b), a shift that ~~ ~~would not have been possible if the source of the LC had become cooler, or if the LC was weakened in order to accommodate the hypothesis of cooling in the shelf~~al~~ area. At the same time, no warming is observed further offshore at DSDP Site 214, strengthening the hypothesis that ~~ODP~~ Site 763~~A~~ tracks the more regional effect of the LC.

Combined, the changes in NSI and paleotemperatures could be explained by an overall long-term increase in water column mixing over the shelf, ~~one that~~which could have been driven by an intensification ~~of seasonality and the related~~ of the atmospheric pressure and steric height gradients over NW Australia. Specifically, ~~s~~Such intensification would translate in stronger trade winds ~~during the winter~~ and LC intensification, a hypothesis that is supported by the observed ~~and~~ warming at ~~ODP~~ Site 763~~A~~. Meanwhile, the decrease in NSI could have been generated either by a sustained increase in vertical mixing and eddy formation over the shelf during the winter season, or by the stronger reversal of the trade winds and monsoonal north-westerlies during the summer, which can promote regional upwelling. Both scenarios, which fall close to a combination of the first and second mechanisms presented in ~~the previous chapter~~section 4.1, could have been the result of an invigoration in seasonal extremes that marked~~, marking~~ the transition to a less tropical, less stratified environment and a significant shift in the paleoecological and paleoceanographic regime in the area (Regime 1 (more stratified, weaker LC) to Regime 2 (less stratified, stronger LC); Figure 7~~8~~). The reverse scenario would apply for the periods before 5.4 Ma and (less intensely) after ~4.2 Ma, when higher NSI and the dominance of *Gephyrocapsa* spp., a bloom-forming group of species with increased tolerance ~~to~~ of warmer and more stratified conditions, is observed. Further offshore, at ~~ODP~~ Site 763~~A~~, where the effect of continental shelf eddy formation and seasonal upwelling is weaker, the invigorated ~~seasonal~~ presence of the LC after ~5.4–5.2 Ma, is solely translated by an overall increase in SSTs.

Although the records investigated in this study do not allow for an extended evaluation of more detailed changes in seasonal dynamics and the ~~the~~ driving mechanisms behind this regime shift, the globally elevated temperatures that marked the

beginning of the Pliocene (~5.3 Ma; Fedorov et al., 2006) could have played a role in increasing monsoonal precipitation and tropical cyclones (Fedorov et al., 2010), therefore invigorating water column mixing in low latitudes. However, this warming was suggested to be an expression of a permanent El Niño state (Fedorov et al., 2006; Wara et al., 2005), which would contradict our argument of an intensified seasonal presence of the LC, since this current is expected to be significantly weaker under such conditions (e.g., Feng et al., 2003, 2009). When compared to other studies, our interpretation falls close to the hypothesis by He and others (2021), namely that the LC was active during the early Pliocene and from 6-4 Ma, before it weakened after ~4 Ma. On the other hand, De Vleeschouwer and others (2022) argued for a strong LC from ~4-3.7 Ma and a weaker phase from ~3.7-3.1 Ma, a reconstruction we cannot evaluate using the NSI because this index cannot be applied after 3.54 Ma (see Figure 43a). More importantly, our study indicates the complex, differential effects that sustained changes in wind and ocean circulation patterns in major currents such as an intensification in seasonality and the LC, would have had on the shelf and further offshore.

4.3 Broader-scale changes in paleoproductivity and paleoecology

Apart from regional ocean circulation patternschanges, the nannofossil assemblages recorded on the NW Australian shelf has the potential tomay reflect broader-scale or even global changespatterns in paleoclimateplankton evolution and variations in the ocean's nutrient budget. On that note, TtThe studied time interval falls within a period of elevated biogenic sedimentation called the late Miocene to early Pliocene biogenic bloom (e.g., Dickens and Owen, 1999; Diester-Haass et al., 2005; Farrell et al., 1995; Hermoyian and Owen, 2001), which has been observed in numerous locations in all major oceans and potentially came to an end, at least in low latitudes, with a sharp decrease in PP that occurred between 4.6–4.4 Ma (Karatsolis et al., 2022). This global event was also expressed at Sites U1463 and U1464 by an abrupt decrease in nannofossil fluxes, as well as a significant restructuring of the nannofossil assemblages, as indicated by the CA (Figure 5) and the increase in H-index (Figure 4b6). Despite the relative abundance changes, small and medium-sized, bloom-forming calcareous nannoplanktoncoccolithophores dominated the assemblage throughout the studied interval. This could partially be explained by the constant supply of nutrients because of a steady terrigenous runoff (Karatsolis et al., 2020) onto the outer shelf/upper bathyal paleoenvironment, where the studied sites were situated during the "Humid Interval" (Christensen et al., 2017; Gallagher et al., 2017). However, it is also in good agreement with a basin-wide eutrophication event, that spanned from ~8.8 Ma (Imai et al., 2015) to ~3.5 Ma; during which *Reticulofenestra haqii* (medium-sized) and *Reticulofenestra minuta* (small small-sized) assemblages dominated in the Indian Ocean (Young, 1990). Within the same period, a *Gephyrocapsa* dominance interval (acme) has been recorded from 4-3 Ma (Young, 1990), consistent with the observed progressive dominance of this species over the NW Australian shelf that followed the termination of the biogenic bloom. However, we can now confirm that a complete dominance overturn was never achieved, as evident by the stepwise increase in diversity H index at 4.6–4.4 Ma (H-index; Figure 4b6), which). This stepwise increase was partly supported by the increase in relative abundances (but not fluxes) of *Calcidiscus* spp. and *Umbilicosphaera* spp. (Figures A2A3, A4, A672, A8)., showing that theseThe latter species taxa were probably affected less by a basin-wide decrease in nutrient availability and mainly mirrored the regional warm

conditions over the shelf. At roughly the same time, large *Reticulofenestra* species virtually disappeared. This falls close to the timing (~5 Ma) of a distinct decrease in the modal size of *Reticulofenestra* species that has been recorded both in the eastern Indian Ocean (ODP Site 757) and the NW Pacific (ODP Site 1201) by Imai et al. (2020), although these authors suggested that the event was restricted to open ocean sites and therefore absent in more coastal locations near the shelf. A trend towards smaller nannofossil sizes continued during the Pliocene (~4–3.8 Ma) ~, indicating an earlier shift towards the period of permanent dominance of smaller-sized placoliths, which has been proposed to have started at ~4–3.8 Ma, with evolutionary innovations events such as the first occurrence (FO) of *Pseudoemiliania* spp. (Figure A10C1) and the LO of *Reticulofenestra pseudoumbilicus* (Aubry, 2007).

Interestingly, Aalthough significant assemblage changes occurred during the PP decrease, there was no major change in NSI (Figure 78). This supports the hypothesis that a broader change decrease in nutrient availability occurred from 4.6–4.4 Ma, one that affected the abundance of dominant species as a whole, and but not the relative ecological success between common taxonomic groups (bloom-forming versus *Sphenolithus*). Additionally, tThe fact that the NSI remained unaltered underpins the potential of this index in decoupling long-term changes in relative dominance of species, controlled by regional ocean circulation patterns and seasonal water column mixing intensity, from large large-scale processes influencing PP through changes in the total ocean nutrient budget.

Further evidence for a decrease in fluxes or significant changes in the nannofossil assemblages, that would have marked the end of the biogenic bloom, are still limited for the rest of the Indian Ocean. Some observations of nannofossil export production from the open ocean ODP HoleSiteSite 757B (Figure 1) support a reduction in burial fluxes in good accordance with our results (Imai et al., 2020). Another study that investigated the nannofossil assemblages at ODP HoleSiteSite 762B (Figure 1), which is located closer to the shelf, recorded a significant decrease in nannofossil fluxes between ~4.2-3.9 Ma, with the nannofossil fluxes returning to higher values after that (Imai et al., 2015). However, it is important to note that the age models of these studies were based on few early Pliocene biostratigraphic tie-points, in contrast to the orbitally-tuned records presented herein. Therefore, the exact timing of events within <0.5 Ma precision should be considered with caution.

As far as it concerns the dominance of small *Gephyrocapsa* is concerned, several acme events of this species have been previously reported during the Pliocene and Pleistocene., but they seem to have been largely diachronous between ocean basins (Auer et al., 2019; Ballegeer et al., 2012; Gibbs et al., 2004; Marino and Flores, 2002). This supports the existence of several controlling mechanisms for the initiation of its dominance, age-model discrepancies, or a non-linear effect of a long-term ecological pressure across basins. Despite the diachronicity, it appears that small *Gephyrocapsa* had an opportunistic advantage in filling the available niches, and a paleoecological advantage to dominate the assemblage in several different paleoenvironments during the early Pliocene. Its increase in relative abundance can already be observed on the NW Australian shelf during, and directly after, the significant reduction in abundance NAR of the opportunistic small *Reticulofenestra* species (4.6–4.4 Ma; Figures A5, A672). However, small *Gephyrocapsa* clearly dominates after 4.2 Ma, and this could be related to our hypothesis of a relative increase in stratification and reduced seasonal mixing of the water column during that time. The subsequent widespread acme in the Indian Ocean (Young, 1990) could have been a result of overall, basin-wide warming and

more stratified conditions, a hypothesis that is supported by the very high early Pliocene temperatures in both open ocean Indian Ocean sites (~~DSDP~~ Sites 214 and ~~; ODP~~ 763~~A~~; Karas et al., 2011) from ~4.3–3.5 Ma. Nevertheless, additional high-

555 resolution nannofossil records are needed to confirm the diachronicity between small *Gephyrocapsa* acme events and the shifts in the nannofossil assemblages that marked the termination of the biogenic bloom.
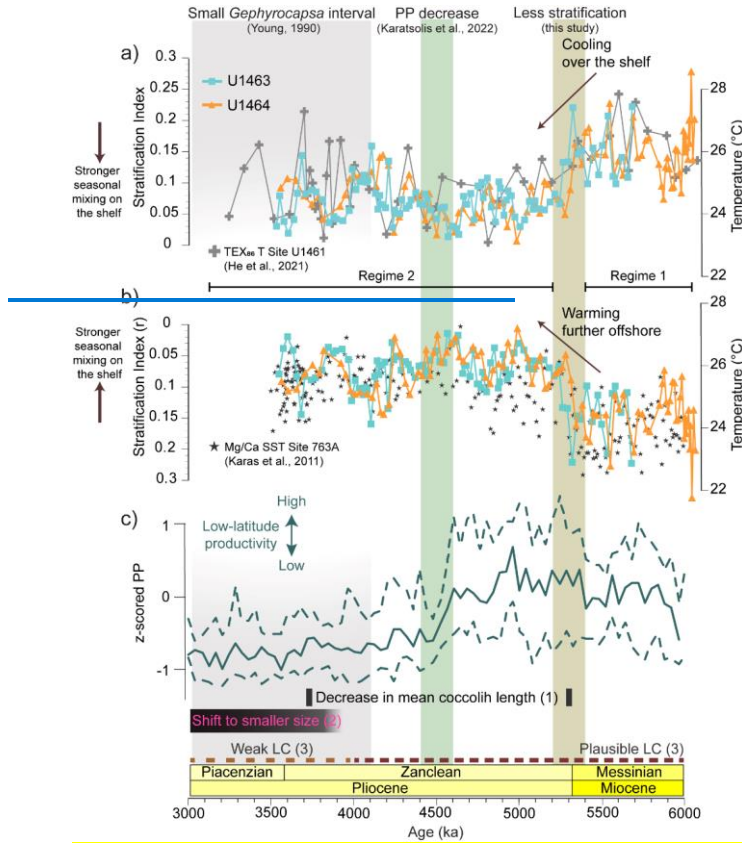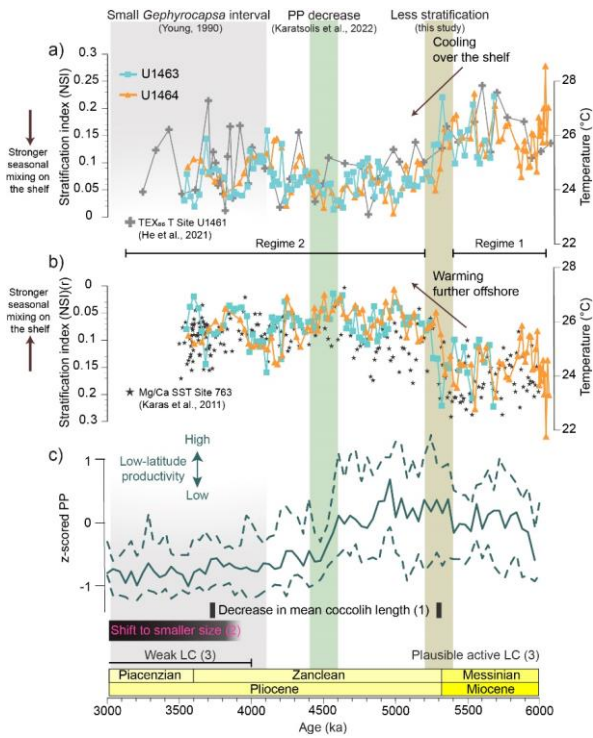
Figure 78. Correlation between paleotemperature proxies for the eastern Indian Ocean, water column stratification over the NW Australian shelf (NSI) and low-latitude paleoproductivity (PP). (**a**) NSI (Nnannofossil stratification index (NSI; see methods) for at IODP Sites U1463 (in light blue) and U1464 (orange) and TEX$_{86}$ derived temperature (°C) at IODP Site U1461 (He et al., 2021), located oin the NW Australian shelf (grey line and crosses). (**b**) NSI (as in panel (**a**), but note reversed (r) scale of y-axis) and *Trilobatus. sacculifer* Mg/Ca-derived (*Trilobatus sacculifer*) SST (°C) at ODP Site 763A (Karas et al., 2011), located near the NW Australian shelf, but further offshore to the west in on the Exmouth Plateau (dark grey stars). Horizontal black lines mark the suggested overall different paleoceanographic regimes before and after the Miocene-Pliocene boundary: Regime 1 with more stratified, stronger LC and Regime 2 with less stratified, stronger LC. (Note reversed scale in y-axis of NSI **c**) Standardised median low latitude PP in low latitudes for in all major ocean basins (Karatsolis et al., 2022). Dashed lines indicate the 15.9 and 84.1 percentiles (i.e. the central 68.2 percentiles) of the compiled data. Horizontal bBlack bars indicate (1) distinct decrease in mean and maximum coccolith length, as recorded in the Indian Ocean (Young, 1990) and, (2) pPeriod of permanent shift to smaller sized coccoliths nannofossils (Aubry 2007); dashed line illustrates (3) Suggested postulated Leeuwin current (LC) LC intensity for the NW Australian shelf area in an earlier study (He et al., 2021). Horizontal black lines indicate the shift from Regime 1 to Regime 2. Vertical shadingsed areas indicate the stepwise decrease in NSI (brown), the decrease in low-latitude paleoproductivity (PP) and nannofossil fluxes over the NW Australian shelf (green) and the small *Gephyrocapsa* dominance interval recorded in the Indian Ocean (greay; Young, 1990).

5. Conclusions

580 During the late Miocene to Pliocene, t~~T~~he NW Australian shelf area ~~during the late Miocene to Pliocene~~ was influenced by an unrestricted ~~Indonesian Throughflow~~ITF and dominated by warm tropical waters under humid climatic conditions. Nannofossil assemblages and paleotemperature gradients between the shelf region and the eastern Indian Ocean ~~Our investigations further~~provide additional ~~constrained~~ constraints on past regional ocean circulation and paleoproductivity between 6-3.5 Ma~~, using the nannofossil assemblage and the paleotemperature gradients between the shelfal area and the~~

585 ~~eastern Indian Ocean~~. The use of a nannofossil stratification index (NSI), which ~~was~~ is based on the abundance of the most common calcareous nannofossil taxonomic groups, revealed a sustained shift in ~~paleoclimatic and~~ paleoceanographic regime across the Miocene-Pliocene boundary, between ~5.4-5.2 Ma. During that time, the water column over the NW Australian shelf transitioned from more stratified, tropical conditions (Regime 1; Figure 7) to a dynamic shelf~~al~~ environment with (seasonally) increased water column mixing and nutrient replenishment in the photic zone (Regime 2; Figure 7). This shift was

590 possibly driven by more pronounced seasonal variations, expressed by intensified storm activity and eddy formation during the winter season and/or enhanced upwelling during the austral summer. The temperature gradients between the shelf~~al~~ area and the pelagic domains of the Indian Ocean, driven by a cooling over the shelf and a warming offshore, further strengthen this interpretation and suggest a more pronounced ~~seasonal~~ flow of the LC after ~5.2 Ma. In addition to regional ocean circulation, we explored the changes in ~~the~~ nannofossil assemblage~~s~~ that characterised the recently proposed termination of

595 the late Miocene to early Pliocene biogenic bloom (4.6-4.4 Ma). Our data suggest that a restructuring of the nannofossil assemblage and an increase in diversity occurred during this interval, although the NSI was not significantly affected. The subsequent dominance of small *Gephyrocapsa* over the NW Australian shelf is interpreted as the expression of the broader dominance of this species in the Indian Ocean and its adaptation to the warm surface water conditions of the early Pliocene. This study highlights the differential response of the nannofossil assemblage to regional ~~seasonal~~ changes in the water column

600 compared to broader-scale changes in paleoproductivity and hypothesized changes in the ocean's nutrient budget ~~in the oceans~~. However, the ~~Questions remain on what~~precise mechanisms that led to the proposed intensification in water column mixing and the possible link to an increase in seasonal~~ity~~ extremes, remain unclear. Furthermore, more research is needed to shed light ~~to and~~on the progressive dominance of small *Gephyrocapsa* during the early Pliocene, as well as the reasons ~~thatwhat caused~~for the changes in ~~the~~ nannofossil assemblage~~s~~ that marked the low-latitude decrease in PP in other ocean basins.

605

Author contributions: B.T.K. conceived the study and performed the nannofossil counts and the data analysis, in close consultation with J.H. B.T.K. interpreted the results and wrote the first draft of this manuscript. J.H. contributed to a critical interpretation and discussion of the results and helped with the writing of the manuscript, ~~and the~~ drafting of the figures and final revisions.

Competing interests: The authors declare that they have no conflict of interest.

Acknowledgements

This research used samples and data provided by the International Ocean Discovery Program and is part of the first author's PhD studies, financially supported by the Swedish Research Council (Vetenskapsrådet; Project Grant VR 2016-04434 to J. H.). We are grateful to the co-chiefs, shipboard science party, and crew of the *JOIDES Resolution* for the successful operations during IODP Expedition 356.

Data availability

Additional data figures and tables that are part of this study can be found in the Appendix section. The raw data produced for this paper are publicly available at the Zenodo data repository (Karatsolis and Henderiks 2022, https://doi.org/10.5281/zenodo.6965870). ~~and have also been submitted to PANGAEA, where they will become available upon publication.~~

630 Figure A1: Latest Miocene to early Pliocene relative abundances (%) of commonly occurring calcareous nannofossil species from IODP Sites U1463 (a-b) and U1464 (c-d). Species are indicated in different colors. Bloom-forming species (<5µm *Reticulofenestra* and <3µm *Gephyrocapsa*; green), small (<3µm) *Reticulofenestra* (red), small (<3µm) *Gephyrocapsa* (blue), *Sphenolithus* spp. (purple), large (>5µm) *Reticulofenestra* (purple-pink), *Umbilicosphaera* spp. (brown) and *Calcidiscus* spp. (orange). Error bars represent 95% confidence intervals (see methods).

635

640

645 **Appendix B: Relative abundance of medium *Reticulofenestra* species plotted against age.**
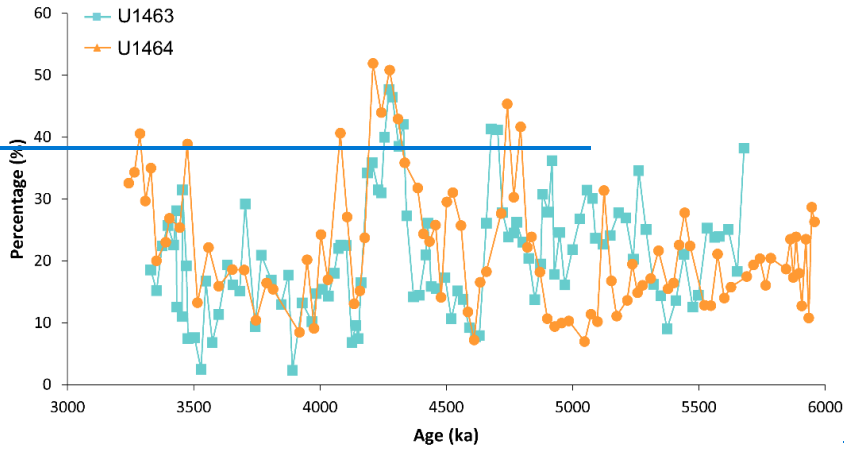
Figure B1: Relative abundances of medium (3-5µm) *Reticulofenestra* species plotted against sample age (ka) at IODP Sites U1463
(open circles; light blue line) and U1464 (closed circles; orange line). Distinct peaks (exceeding 40% of the assemblage) can be
650 **observed shortly before (~4.7 Ma) and after (~4.3 Ma) the 4.6–4.4 Ma decrease in PP.**

660

665

Figure A1~~:~~ Latest Miocene to early Pliocene relative abundances (%) of the dominant calcareous nannofossil species ~~from~~at IODP Site~~s~~ U1463 ~~(A–D)~~. **(a)** Bloom-forming species (<5μm *Reticulofenestra* and <3μm *Gephyrocapsa* combined; green circles), **(b)** small (<3μm) *Reticulofenestra* (red triangles), **(c)** small (<3μm) *Gephyrocapsa* (blue plus signs), **(d)** *Sphenolithus* spp. (purple crosses). Shaded areas represent 95% confidence intervals (see methods). Note different y-axis scale in panel **(d)**. ~~Species are indicated in different colors. Bloom-forming species (<5μm *Reticulofenestra* and <3μm *Gephyrocapsa*; green circles), small (<3μm) *Reticulofenestra* (red triangles), small (<3μm) *Gephyrocapsa* (blue crosses), *Sphenolithus* spp. (purple x-signs). Shaded areas represent 95% confidence intervals (see methods). Note different y-axis values in panel D.~~

675
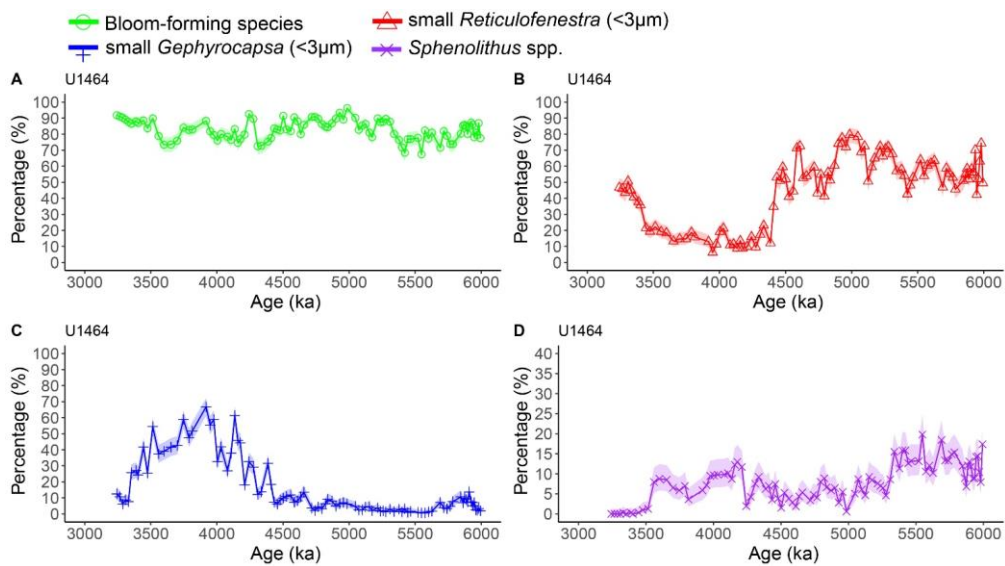
Figure A2. Latest Miocene to early Pliocene relative abundances (%) of the dominant calcareous nannofossil species at IODP
680 Site U1464. **(a)** Bloom-forming species (<5μm *Reticulofenestra* and <3μm *Gephyrocapsa* combined; green circles), **(b)** small
(<3μm) *Reticulofenestra* (red triangles), **(c)** small (<3μm) *Gephyrocapsa* (blue plus signs), **(d)** *Sphenolithus* spp. (purple
crosses). Shaded areas represent 95% confidence intervals (see methods). Note different y-axis scale in panel **(d)**.

Formatted: Font: Not Bold
Formatted: Font: Not Bold
Formatted: Font: Not Bold
Formatted: Font: Not Bold
Formatted: Font: Not Bold
Formatted: Font: Not Bold
Formatted: Justified
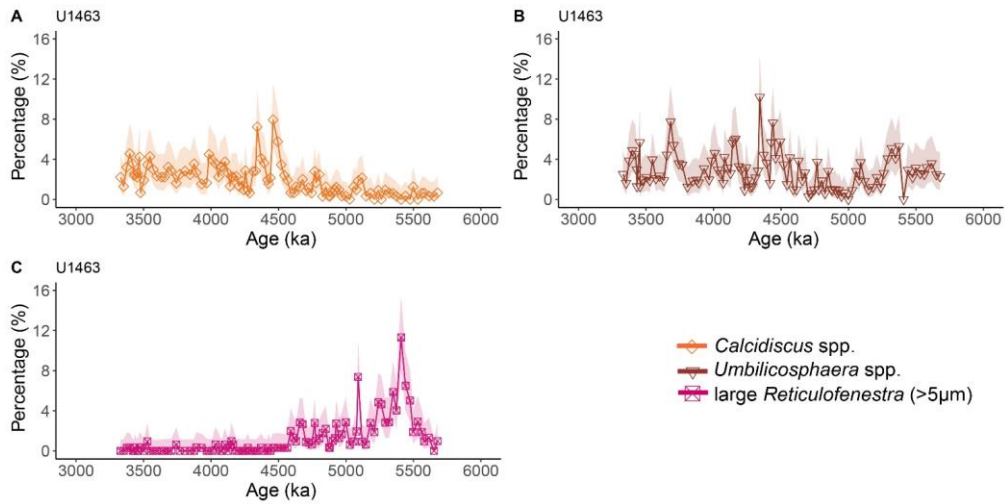
685 **Figure A3** Latest Miocene to early Pliocene relative abundances (%) of common calcareous nannofossil species at IODP Site U1463. **(a)** *Calcidiscus* spp. (orange diamonds), **(b)** *Umbilicosphaera* spp. (brown triangles) and **(c)** large (>5μm) *Reticulofenestra* (purple-pink squares). Shaded areas represent 95% confidence intervals (see methods).

690
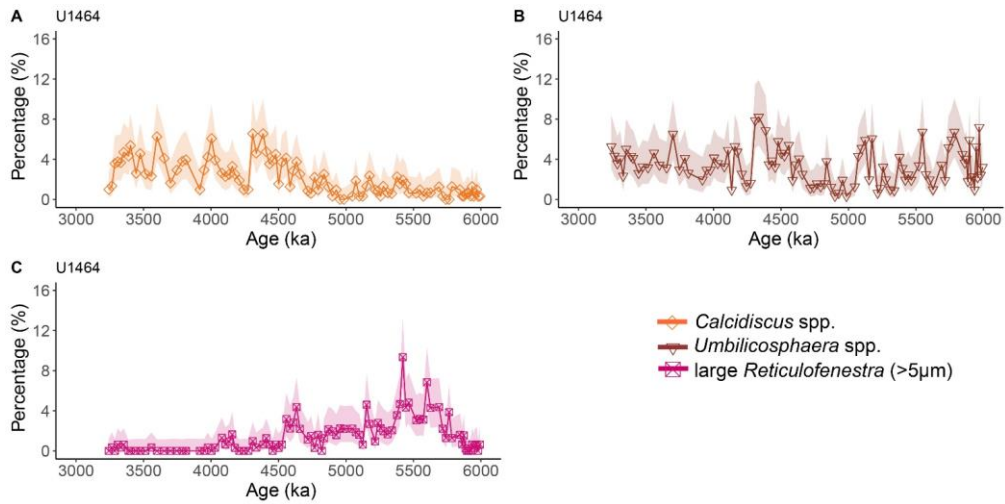
Figure A4 Latest Miocene to early Pliocene relative abundances (%) of common calcareous nannofossil species at IODP Site U1464. **(a)** *Calcidiscus* spp. (orange diamonds), **(b)** *Umbilicosphaera* spp. (brown triangles) and **(c)** large (>5µm) *Reticulofenestra* (purple-pink squares). Shaded areas represent 95% confidence intervals (see methods).
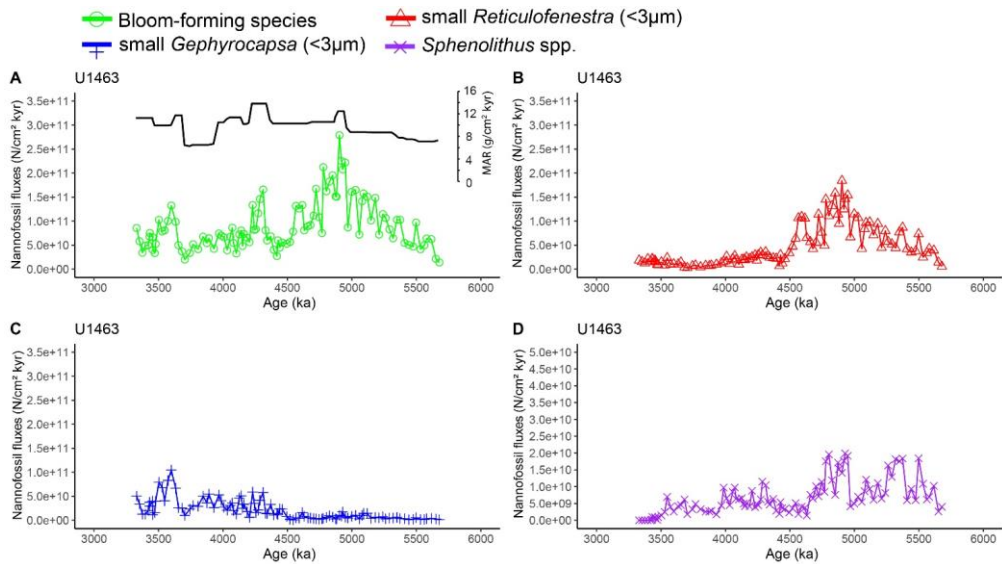
700 **Figure A5** Latest Miocene to early Pliocene nannofossil fluxes (NAR; N/cm^2 kyr) of commonly occurring calcareous nannofossil species at IODP Site U1463. **(a)** Bloom-forming species (<5μm *Reticulofenestra* and <3μm *Gephyrocapsa*; green circles), with inset bulk sediment MAR (g/cm^2 kyr) (black line); **(b)** small (<3μm) *Reticulofenestra* (red triangles), **(c)** small (<3μm) *Gephyrocapsa* (blue plus signs), **(d)** *Sphenolithus* spp. (purple crosses). Error bars of maximum replication error (15%; (Bordiga et al., 2015) were too small and therefore impaired the visual inspection of the figure. However, they are available as 705 part of the source data of the paper. Note different y-axis scale in panel **(d)**.

Figure A6 Latest Miocene to early Pliocene nannofossil fluxes (NAR; N/cm^2 kyr) of commonly occurring calcareous nannofossil species at IODP Site U1464. **(a)** Bloom-forming species (<5μm *Reticulofenestra* and <3μm *Gephyrocapsa*; green circles), with inset bulk sediment MAR (g/cm^2 kyr) (black line), **(b)** small (<3μm) *Reticulofenestra* (red triangles), **(c)** small (<3μm) *Gephyrocapsa* (blue plus signs), **(d)** *Sphenolithus* spp. (purple crosses). Error bars of maximum replication error (15%; (Bordiga et al., 2015) were too small and therefore impaired the visual inspection of the figure. However, they are available as part of the source data of the paper. Note different y-axis scale in panel **(d)**.

Figure A67: Latest Miocene to early Pliocene nNannofossil ~~Accumulation Rates~~fluxes (NAR; N/cm² kyr) of commonly occurring calcareous nannofossil species ~~from~~at IODP Site U1463 ~~(A-C). Species are indicated in different colors~~. **(a)** *Calcidiscus* spp. (orange ~~rhombi~~diamonds), **(b)** *Umbilicosphaera* spp. (brown ~~reverse~~ triangles) and **(c)** large (>5µm) *Reticulofenestra* (purple-pink squares ~~with x-signs~~). Error bars of maximum replication error (±15%; (Bordiga et al., 2015) were too small and therefore impaired the visual inspection of the figure. However, they are available as part of the source data of thi~~s~~e paper.

725
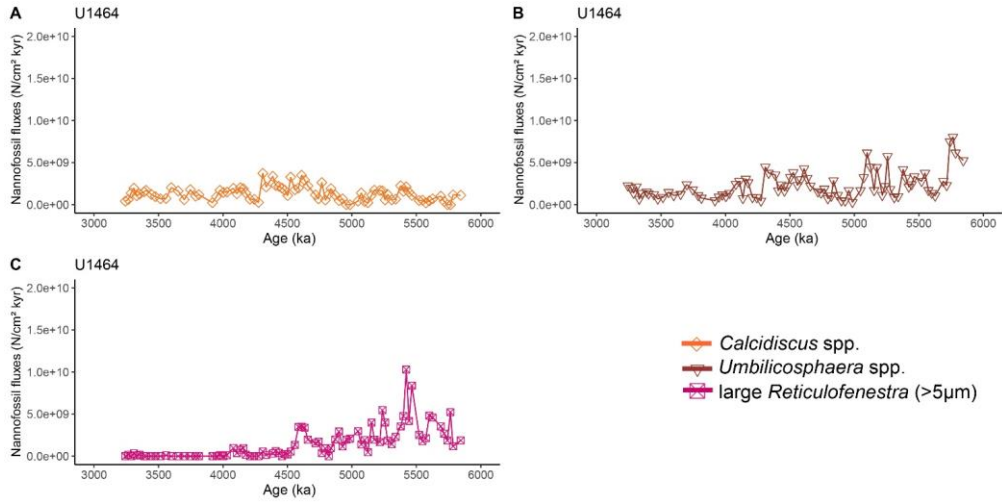
Figure A8: Latest Miocene to early Pliocene nNannofossil Accumulation Ratesfluxes (NAR; N/cm² kyr) of commonly occurring calcareous nannofossil species fromat IODP Site U1464 (A-C). Species are indicated in different colors. **(a)** *Calcidiscus* spp. (orange rhombidiamonds), **(b)** *Umbilicosphaera* spp. (brown reverse triangles) and **(c)** large (>5µm) *Reticulofenestra* (purple-pink squares with x signs). Error bars of maximum replication error (±15%; (Bordiga et al., 2015) were too small and therefore impaired the visual inspection of the figure. However, they are available as part of the source data of thethis paper.

735
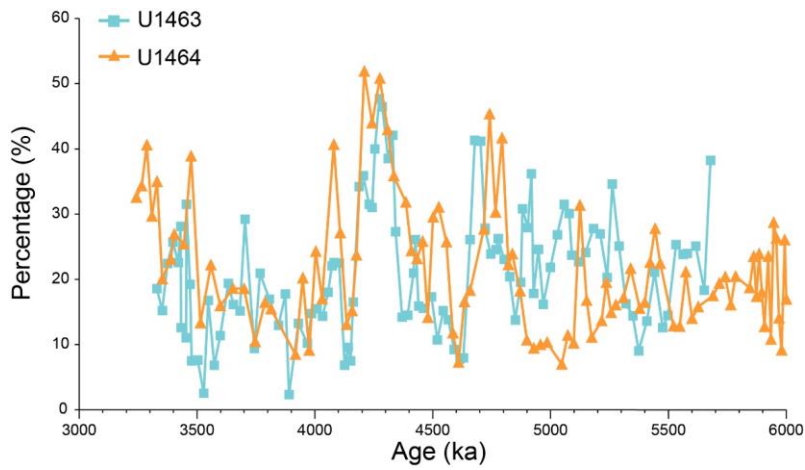
Figure A9: Relative abundances (%) of medium-sized (3-5μm) *Reticulofenestra* species plotted against sample age (ka) at IODP Sites U1463 (light blue squares) and U1464 (orange triangles). Distinct peaks (exceeding 40% of the assemblage) can be observed shortly before (~4.7 Ma) and after (~4.3 Ma) the 4.6–4.4 Ma decrease in PP.

740
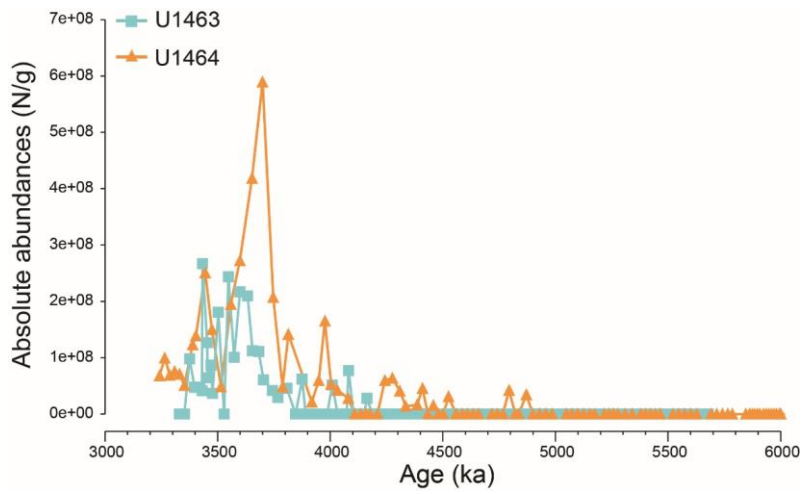
Figure A10: Absolute coccolith abundances (N/g × 10⁸) of *Pseudoemiliania lacunosa* plotted against sample age (ka) at IODP Sites U1463 (light blue squares) and U1464 (orange triangles).

745

Appendix ~~D~~ Summary of median age and temperature differences for the ~~c~~Palculated paleotemperature gradients.

Table ~~A~~D1~~:~~ Summary of median differences in sample age (Δage, kyr) and paleotemperature (ΔT, °C) ~~differences~~ for the calculated gradients between eastern Indian Ocean and NW Australian shelf sites. ~~Initial~~ Input data ~~records represent~~ are alkenone- ($U_{37}^{k'}$) and GDGT-based (TEX$_{86}$) temperature estimates from IODP Site U1461 (He et al., 2021) and planktonic foraminifera-based (Mg/Ca) SST estimates for ODP Site 763~~A~~ (Karas et al., 2011) and DSDP Site 214 (Karas et al., 2009).

760

Gradient (Sites)	Median Δage* (kyr) 6-3.5 Ma	Median ΔT (°C) 5.2-3.5 Ma	Median ΔT (°C) 6-5.2 Ma
U1461 ($U_{37}^{k'}$)-763 (Mg/Ca)	2.8	-0.2	
U1461 ($U_{37}^{k'}$)-214 (Mg/Ca)	9.6	-0.5	
U1461 (TEX$_{86}$)-763 (Mg/Ca)	2.9	-0.6	2
U1461 (TEX$_{86}$)-214 (Mg/Ca)	7.8	-1.15	

*Median Δage is calculated from the absolute difference between IODP Site U1461 sample ages and the closest available sample ages from ODP Site 763/DSDP Site 214

765 **References**

Anand, P., Elderfield, H., and Conte, M. H: Calibration of Mg/Ca thermometry in planktonic foraminifera from a sediment trap time series, Paleoceanography, 18(2), 1050, doi:10.1029/2002PA000846, 2003.

Aubry, M.-P.: A major Pliocene coccolithophore turnover: Change in morphological strategy in the photic zone, Geol. Soc. Am., 424, 51, doi:https://doi.org/10.1130/SPE424, 2007.

770 Auer, G., De Vleeschouwer, D., Smith, R. A., Bogus, K., Groeneveld, J., Grunert, P., Castañeda, I. S., Petrick, B., Christensen, B., Fulthorpe, C., Gallagher, S. J. and Henderiks, J.: Timing and Pacing of Indonesian Throughflow Restriction and Its Connection to Late Pliocene Climate Shifts, Paleoceanogr. Paleoclimatology, 34(4), 635–657, doi:10.1029/2018PA003512, 2019.

Auer, G., Petrick, B., Yoshimura, T., Mamo, B. L., Reuning, L., Takayanagi, H., De Vleeschouwer, D. and Martinez-Garcia,
775 A.: Intensified organic carbon burial on the Australian shelf after the Middle Pleistocene transition, Quat. Sci. Rev., 262, 106965, doi:10.1016/j.quascirev.2021.106965, 2021.

Ballegeer, A. M., Flores, J. A., Sierro, F. J. and Andersen, N.: Monitoring fluctuations of the Subtropical Front in the Tasman Sea between 3.45 and 2.45 Ma (ODP site 1172), Palaeogeogr. Palaeoclimatol. Palaeoecol., 313–314, 215–224, doi:10.1016/j.palaeo.2011.11.001, 2012.

780 Beaufort, L., Lancelot, Y., Camberlin, P., Cayre, O., Vincent, E., Bassinot, F. and Labeyrie, L.: Insolation cycles as a major control of equatorial Indian Ocean primary production, Science, (80-.)., 278(5342), 1451–1454, doi:10.1126/science.278.5342.1451, 1997.

Boeckel, B. and Baumann, K.-H.: Vertical and lateral variations in coccolithophore community structure across the subtropical frontal zone in the South Atlantic Ocean, Mar. Micropaleontol., 67(3–4), 255–273, doi:10.1016/j.marmicro.2008.01.014, 2008.

785 Bolton, C. T., Hernández-Sánchez, M. T., Fuertes, M. Á., González-Lemos, S., Abrevaya, L., Mendez-Vicente, A., Flores, J. A., Probert, I., Giosan, L., Johnson, J. and Stoll, H. M.: Decrease in coccolithophore calcification and CO$_2$ since the middle Miocene, Nat. Commun., 7, doi:10.1038/ncomms10284, 2016.

Bordiga, M., Bartol, M. and Henderiks, J.: Absolute nannofossil abundance estimates: Quantifying the pros and cons of different techniques, Rev. Micropaleontol., 58(3), 155–165, doi:10.1016/j.revmic.2015.05.002, 2015.

790 Bralower, T. J.: Evidence of surface water oligotrophy during the Paleocene-Eocene thermal maximum: Nannofossil assemblage data from Ocean Drilling Program Site 690, Maud Rise, Weddell Sea, Paleoceanography, 17(2), 583–592, doi:10.1029/2001pa000662, 2002.

Chen, M., Pattiaratchi, C. B., Ghadouani, A. and Hanson, C.: Influence of Storm Events on Chlorophyll Distribution Along the Oligotrophic Continental Shelf Off South-Western Australia, Front. Mar. Sci., 7(May), 1–19,
795 doi:10.3389/fmars.2020.00287, 2020.

Christensen, B. A., Renema, W., Henderiks, J., De Vleeschouwer, D., Groeneveld, J., Castañeda, I. S., Reuning, L., Bogus, K., Auer, G., Ishiwa, T., McHugh, C. M., Gallagher, S. J., Fulthorpe, C. S., Mamo, B. L., Kominz, M. A., McGregor, H. V., Petrick, B. F., Takayanagi, H., Levin, E., Korpanty, C. A., Potts, D. C., Baranwal, S., Franco, D. R., Gurnis, M., Haller, C., He, Y., Himmler, T., Iwatani, H., Jatiningrum, R. S., Lee, E. Y., Rastigar, A. and Zhang, W.: Indonesian Throughflow drove
800 Australian climate from humid Pliocene to arid Pleistocene, Geophys. Res. Lett., 44(13), 6914–6925, doi:10.1002/2017GL072977, 2017.

D'Adamo, N., Fandry, C., Buchan, S. and Domingues, C.: Northern sources of the Leeuwin Current and the "Holloway Current" on the North West Shelf, J. R. Soc. West. Aust., 92(2), 53–66, 2009.

De Vleeschouwer, D., Petrick, B. F. and Martínez-García, A.: Stepwise Weakening of the Pliocene Leeuwin Current, Geophys.
805 Res. Lett., 46(14), 8310–8319, doi:10.1029/2019GL083670, 2019.

De Vleeschouwer, D., Peral, M., Marchegiano, M., Füllberg, A., Meinicke, N., Pälike, H., Auer, G., Petrick, B., Snoeck, C.,

Goderis, S. and Claeys, P.: Plio-Pleistocene Perth Basin water temperatures and Leeuwin Current dynamics (Indian Ocean) derived from oxygen and clumped-isotope paleothermometry, Clim. Past, 18(5), 1231–1253, doi:10.5194/cp-18-1231-2022, 2022.

810   Dekens, P. S., Lea, D. W., Pak, D. K., and Spero, H. J.: Core top calibration of Mg/Ca in tropical foraminifera: Refining paleotemperature estimation, Geochem. Geophys. Geosyst., 3(4), doi:10.1029/2001GC000200, 2002.

Dickens, G. R. and Owen, R. M.: The Latest Miocene-Early Pliocene biogenic bloom: A revised Indian Ocean perspective, Mar. Geol., 161(1), 75–91, doi:10.1016/S0025-3227(99)00057-2, 1999.

Diester-Haass, L., Billups, K. and Emeis, K. C.: In search of the late Miocene-early Pliocene "biogenic bloom" in the Atlantic
815   Ocean (Ocean Drilling Program Sites 982, 925, and 1088), Paleoceanography, 20(4), 1–13, doi:10.1029/2005PA001139, 2005.

Du, Y. and Qu, T.: Three inflow pathways of the Indonesian throughflow as seen from the simple ocean data assimilation, Dyn. Atmos. Ocean., 50(2), 233–256, doi:10.1016/j.dynatmoce.2010.04.001, 2010.

Eglinton, T. I., Conte, M. H., Eglinton, G., and Hayes, J. M.: Proceedings of a workshop on alkenone-based paleoceanographic indicators, Geochem. Geophys. Geosyst., 2, 1031, doi:10.1029/2000GC000122, 2001.

820   Farrell, J. W., Raffi, I, Janecek, T. C., Murray, D. W., Levitan, M., Dadey, K. A., Emeis, K.-C., Lyle, M., Flores, J.-A. and Hovan, S.: Late Neogene Sedimentation Patterns in the Eastern Equatorial Pacific, Proc. Ocean Drill. Program, 138 Sci. Results, (August), doi:10.2973/odp.proc.sr.138.143.1995, 1995.

Fedorov, A. V., Dekens, P. S., McCarthy, M., Ravelo, A. C., DeMenocal, P. B., Barreiro, M., Pacanowski, R. C. and Philander, S. G.: The Ppliocene paradox (mechanisms for a permanent El Niño), Science (80-.)., 312(5779), 1485–1489,
825   doi:10.1126/science.1122666, 2006.

Fedorov, A. V., Brierley, C. M. and Emanuel, K.: Tropical cyclones and permanent El Niño in the early Ppliocene epoch, Nature, 463(7284), 1066–1070, doi:10.1038/nature08831, 2010.

Feng, M., Meyers, G., Pearce, A. and Wijffels, S.: Annual and interannual variations of the Leeuwin Current at 32°S, J. Geophys. Res. Ocean., 108(11), doi:10.1029/2002jc001763, 2003.

830   Feng, M., Waite, A. M. and Thompson, P. A.: Climate variability and ocean production in the Leeuwin Current system off the west coast of Western Australia, J. R. Soc. West. Aust., 92(2), 67–81, 2009.

Flores, J. A., Bárcena, M. A. and Sierro, F. J.: Ocean-surface and wind dynamics in the Atlantic Ocean off Northwest Africa during the last 140—000 years, Palaeogeogr. Palaeoclimatol. Palaeoecol., 161(3–4), 459–478, doi:10.1016/S0031-0182(00)00099-7, 2000.

835   Furnas, M.: Intra-seasonal and inter-annual variations in phytoplankton biomass, primary production and bacterial production at North West Cape, Western Australia: Links to the 1997-1998 El Niño event, Cont. Shelf Res., 27(7), 958–980, doi:10.1016/j.csr.2007.01.002, 2007.

Gallagher, S. J., Wallace, M. W., Li, C. L., Kinna, B., Bye, J. T., Akimoto, K. and Torii, M.: Neogene history of the West Pacific Warm Pool, Kuroshio and Leeuwin currents, Paleoceanography, 24(1), doi:10.1029/2008PA001660, 2009.

840   Gallagher, S. J., Fulthorpe, C. S., Bogus, K., Auer, G., Baranwal, S., Castañeda, I. S., Christensen, B. A., De Vleeschouwer, D., Franco, D. R., Groeneveld, J., Gurnis, M., Haller, C., He, Y., Henderiks, J., Himmler, T., Ishiwa, T., Iwatani, H., Jatiningrum, R. S., Kominz, M. A., Korpanty, C. A., Lee, E. Y., Levin, E., Mamo, B. L., McGregor, H. V., McHugh, C. M., Petrick, B. F., Potts, D. C., Rastegar Lari, A., Renema, W., Reuning, L., Takayanagi, H. and Zhang, W.: Expedition 356 summary, , 356(February), doi:10.14379/iodp.proc.356.101.2017, 2017.

845   Gallagher, S.J., Fulthorpe, C.S., Bogus, K., Auer, G., Baranwal, S., Castañeda, I.S., Christensen, B.A., De Vleeschouwer, D., Franco, D.R., Groeneveld, J., Gurnis, M., Haller, C., He, Y., Henderiks, J., Himmler, T., Ishiwa, T., Iwatani, H., Jatiningrum, R.S., Kominz, M.A., Korpanty, C.A., Lee, E.Y., Levin, E., Mamo, B.L., McGregor, H.V., McHugh, C.M., Petrick, B.F., Potts, D.C., Rastegar Lari, A., Renema, W., Reuning, L., Takayanagi, H., and Zhang, W.: Expedition 356 summary. In Gallagher, S.J., Fulthorpe, C.S., Bogus, K., and the Expedition 356 Scientists, Indonesian Throughflow. Proceedings of the International

Ocean Discovery Program, 356: College Station, TX (International Ocean Discovery Program). http://dx.doi.org/10.14379/iodp.proc.356.101.2017, 2017

Gallagher, S.J., Fulthorpe, C.S., Bogus, K., Auer, G., Baranwal, S., Castañeda, I.S., Christensen, B.A., De Vleeschouwer, D., Franco, D.R., Groeneveld, J., Gurnis, M., Haller, C., He, Y., Henderiks, J., Himmler, T., Ishiwa, T., Iwatani, H., Jatiningrum, R.S., Kominz, M.A., Korpanty, C.A., Lee, E.Y., Levin, E., Mamo, B.L., McGregor, H.V., McHugh, C.M., Petrick, B.F., Potts, D.C., Rastegar Lari, A., Renema, W., Reuning, L., Takayanagi, H., and Zhang, W.: Site U1463. In Gallagher, S.J., Fulthorpe, C.S., Bogus, K., and the Expedition 356 Scientists, Indonesian Throughflow. Proceedings of the International Ocean Discovery Program, 356: College Station, TX (International Ocean Discovery Program). http://dx.doi.org/10.14379/iodp.proc.356.108.2017, 2017.

Gallagher, S.J., Fulthorpe, C.S., Bogus, K., Auer, G., Baranwal, S., Castañeda, I.S., Christensen, B.A., De Vleeschouwer, D., Franco, D.R., Groeneveld, J., Gurnis, M., Haller, C., He, Y., Henderiks, J., Himmler, T., Ishiwa, T., Iwatani, H., Jatiningrum, R.S., Kominz, M.A., Korpanty, C.A., Lee, E.Y., Levin, E., Mamo, B.L., McGregor, H.V., McHugh, C.M., Petrick, B.F., Potts, D.C., Rastegar Lari, A., Renema, W., Reuning, L., Takayanagi, H., and Zhang, W.: Site U1464. In Gallagher, S.J., Fulthorpe, C.S., Bogus, K., and the Expedition 356 Scientists, Indonesian Throughflow. Proceedings of the International Ocean Discovery Program, 356: College Station, TX (International Ocean Discovery Program). http://dx.doi.org/10.14379/iodp.proc.356.109.2017, 2017.

Gibbs, S., Shackleton, N. and Young, J.: Orbitally forced climate signals in mid-Pliocene nannofossil assemblages, Mar. Micropaleontol., 51(1–2), 39–56, doi:10.1016/j.marmicro.2003.09.002, 2004.

Gibbs, S. J., Young, J. R., Bralower, T. J. and Shackleton, N. J.: Nannofossil evolutionary events in the mid-Pliocene: An assessment of the degree of synchrony in the extinctions of *Reticulofenestra pseudoumbilicus* and *Sphenolithus abies*, Palaeogeogr. Palaeoclimatol. Palaeoecol., 217(1–2), 155–172, doi:10.1016/j.palaeo.2004.11.005, 2005.

Gibbs, S. J., Stoll, H. M., Bown, P. R. and Bralower, T. J.: Ocean acidification and surface water carbonate production across the Paleocene-Eocene thermal maximum, Earth Planet. Sci. Lett., 295(3–4), 583–592, doi:10.1016/j.epsl.2010.04.044, 2010.

Godfrey, J. S.: The effect of the Indonesian throughflow on ocean circulation and heat exchange with the atmosphere: A review, J. Geophys. Res. Ocean., 101(C5), 12217–12237, doi:10.1029/95JC03860, 1996.

Godfrey, J. S. and Ridgway, K. R.: The Large-Scale Environment of the Poleward-Flowing Leeuwin Current, Western Australia: Longshore Steric Height Gradients, Wind Stresses and Geostrophic Flow, J. Phys. Oceanogr., 15(5), 481–495, doi:10.1175/1520-0485(1985)015<0481:TLSEOT>2.0.CO;2, 1985.

Godfrey, J. S., Vaudrey, D. J. and Hahn, S. D.: Observations of the Shelf-Edge Current South of Australia, Winter 1982, J. Phys. Oceanogr., 16(4), 668–679, doi:10.1175/1520-0485(1986)016<0668:OOTSEC>2.0.CO;2, 1986.

Gordon, A. L., Ma, S., Olson, D. B., Hacker, P., Ffield, A., Talley, L. D., Wilson, D. and Baringer, M.: Advection and diffusion of Indonesian throughflow water within the Indian Ocean South Equatorial Current, Geophys. Res. Lett., 24(21), 2573–2576, doi:10.1029/97GL01061, 1997.

Gradstein, F. M., Ogg, J. G., Schmitz, M. D., and Ogg, G. M. (Eds): The Geologic Time Scale 2012 (Vol. 2, p. 1144). Amsterdam: Elsevier, 2012.

Groeneveld, J., De Vleeschouwer, D., McCaffrey, J. C. and Gallagher, S. J.: Dating the Northwest Shelf of Australia since the Pliocene, Geochemistry, Geophys. Geosystems, 22(3), 1–20, doi:10.1029/2020GC009418, 2021.

Hammer, Ø., Harper, D. A. T. and Ryan, P. D.: PAST: Paleontological Statistics Software Package for education and data analysis., , 4, 1–9, 2001.

Hannisdal, B., Henderiks, J. and Liow, L. H.: Long-term evolutionary and ecological responses of calcifying phytoplankton to changes in atmospheric CO_2, Glob. Chang. Biol., 18(12), 3504–3516, doi:10.1111/gcb.12007, 2012.

Haq, B. U.: Biogeographic history of Miocene calcareous nannoplankton and paleoceanography of the Atlantic Ocean.,

Micropaleontology, 26(4), 414–443, doi:10.2307/1485353, 1980.

Haq, B. U. and Lohmann, G. P.: Early Cenozoic calcareous nannoplankton biogeography of the Atlantic Ocean, Mar. Micropaleontol., 1, 119–194, 10.1016/0377-8398(76)90008-6 , 1976.

Harlay, J., Borges, A. V., Van Der Zee, C., Delille, B., Godoi, R. H. M., Schiettecatte, L. S., Roevros, N., Aerts, K., Lapernat, P. E., Rebreanu, L., Groom, S., Daro, M. H., Van Grieken, R. and Chou, L.: Biogeochemical study of a coccolithophore bloom in the northern Bay of Biscay (NE Atlantic Ocean) in June 2004, Prog. Oceanogr., 86(3–4), 317–336, doi:10.1016/j.pocean.2010.04.029, 2010.

Harris, G., Nilsson, C., Clementson, L. and Thomas, D.: The water masses of the east coast of Tasmania: Seasonal and interannual variability and the influence on phytoplankton biomass and productivity, Aust. J. Mar. Freshw. Res., 38(5), 569–590, doi:10.1071/MF9870569, 1987.

He, Y., Wang, H. and Liu, Z.: Development of the Leeuwin Current on the northwest shelf of Australia through the Pliocene-Pleistocene period, Earth Planet. Sci. Lett., 559, 116767, doi:10.1016/j.epsl.2021.116767, 2021.

Henderiks, J., Bartol, M., Pige, N., Karatsolis, B. T. and Lougheed, B. C.: Shifts in Phytoplankton Composition and Stepwise Climate Change During the Middle Miocene, Paleoceanogr. Paleoclimatology, 35(8), doi:10.1029/2020PA003915, 2020.

Hermoyian, C. S. and Owen, R. M.: Late Miocene-early Pliocene biogenic bloom: Evidence from low-productivity regions of the Indian and Atlantic oceans, Paleoceanography, 16(1), 95–100, doi:10.1029/2000PA000501, 2001.

Hirst, G. and Godfrey, J. S.: The Role of Indonesian Throughflow in a Global Ocean GCM, J. Phys. Oceanogr., 23(6), 1057–1086, doi:10.1175/1520-0485(1993)023<1057:TROITI>2.0.CO;2, 1993.

Holloway, P. E. and Nye, H.: Leeuwin current and wind distributions on the southern part of the Australian North West Shelf between January 1982 and July 1983, Mar. Freshw. Res., 36, 123–137, 10.1071/MF9850123, 1985.

Imai, R., Farida, M., Sato, T. and Iryu, Y.: Evidence for eutrophication in the northwestern Pacific and eastern Indian oceans during the Miocene to Pleistocene based on the nannofossil accumulation rate, *Discoaster* abundance, and coccolith size distribution of *Reticulofenestra*, Mar. Micropaleontol., 116, 15–27, doi:10.1016/j.marmicro.2015.01.001, 2015.

Imai, R., Sato, T., Chiyonobu, S. and Iryu, Y.: Reconstruction of Miocene to Pleistocene sea-surface conditions in the eastern Indian Ocean on the basis of calcareous nannofossil assemblages from ODP Hole 757B, Isl. Arc, 29(1), doi:10.1111/iar.12373, 2020.

Karas, C., Nürnberg, D., Gupta, A. K., Tiedemann, R., Mohan, K. and Bickert, T.: Mid-Pliocene climate change amplified by a switch in Indonesian subsurface throughflow, Nat. Geosci., 2(6), 434–438, doi:10.1038/ngeo520, 2009.

Karas, C., Nürnberg, D., Tiedemann, R. and Garbe-Schönberg, D.: Pliocene Indonesian Throughflow and Leeuwin Current dynamics: Implications for Indian Ocean polar heat flux, Paleoceanography, 26(2), 1–9, doi:10.1029/2010PA001949, 2011.

Karatsolis, B.-Th. and Henderiks, J., (2022). Late Miocene to Pliocene calcareous nannofossil assemblage records and paleotemperature gradients from the NW Australian shelf (IODP Sites U1463, U1464) [Data set]. https://doi.org/10.5281/zenodo.6965870

Karatsolis, B.-Th., Lougheed, B. C., De Vleeschouwer, D. and Henderiks, J.: Abrupt conclusion of the late Miocene-early Pliocene biogenic bloom at 4.6-4.4 Ma, Nat. Commun., 13(1), 1–9, doi:10.1038/s41467-021-27784-6, 2022.

Karatsolis, B.-Th., De Vleeschouwer, D., Groeneveld, J., Christensen, B. and Henderiks, J.: The Late Miocene to Early Pliocene "Humid Interval" on the NW Australian Shelf: Disentangling climate forcing from regional basin evolution, Paleoceanogr. Paleoclimatology, 35(9), doi:10.1029/2019PA003780, 2020.

Kendrick, G. A., Goldberg, N. A., Harvey, E. S. and McDonald, J.: Historical and contemporary influence of the Leeuwin Current on the marine biota of the southwestern Australian continental shelf and the Recherche Archipelago, J. R. Soc. West. Aust., 92(2), 211–219, 2009.

Kim, J-H., Villanueva, L., Zell, C., and Sinninghe Damsté, J. S.: Biological source and provenance of deep-water derived

935   isoprenoid tetraether lipids along the Portuguese continental margin,Geoch. et Cosmoch. Acta, 172, 177-204, doi:10.1016/j.gca.2015.09.010, 2016.

Kimura, S., Nakata, H. and Okazaki, Y.: Biological production in meso-scale eddies caused by frontal disturbances of the Kuroshio Extension, ICES J. Mar. Sci., 57(1), 133–142, doi:10.1006/jmsc.1999.0564, 2000.

Koch, C. and Young, J. R.: A simple weighing and dilution technique for determining absolute abundances of coccoliths from
940   sediment samples, J. Nannoplankt. Res., 29(1), 67–69, 2007.

Koslow, J. A., Pesant, S., Feng, M., Pearce, A., Fearns, P., Moore, T., Matear, R. and Waite, A.: The effect of the Leeuwin Current on phytoplankton biomass and production off Southwestern Australia, J. Geophys. Res. Ocean., 113(7), doi:10.1029/2007JC004102, 2008.

Longhurst, A.: A major seasonal phytoplankton bloom in the Madagascar Basin, Deep. Res. Part I Oceanogr. Res. Pap., 48(11),
945   2413–2422, doi:10.1016/S0967-0637(01)00024-3, 2001.

Marino, M. and Flores, J. A.: Miocene to Pliocene calcareous nannofossil biostratigraphy at ODP Leg 177 Sites 1088 and 1090, Mar. Micropaleontol., 45(3–4), 291–307, doi:10.1016/S0377-8398(02)00033-6, 2002.

Müller, P., J., Kirst, G., Ruhland, G., von Storch, I. and Rosell-Melé, A.: Calibration of the alkenone paleotemperature index $U^{k'}_{37}$ based on core-tops from the eastern South Atlantic and the global ocean (60°N-60°S), Geochim. Cosmochim. Acta, 62
950   (10), 1757-1772, doi:10.1016/S0016-7037(98)00097-0, 1998.

O'Dea, S. A., Gibbs, S. J., Bown, P. R., Young, J. R., Poulton, A. J., Newsam, C. and Wilson, P. A.: Coccolithophore calcification response to past ocean acidification and climate change, Nat. Commun., 5, 1–7, doi:10.1038/ncomms6363, 2014.

Okada, H. and Wells, P.: Late quaternary nannofossil indicators of climate change in two deep-sea cores associated with the Leeuwin Current off Western Australia, Palaeogeogr. Palaeoclimatol. Palaeoecol., 131(3–4), 413–432, doi:10.1016/S0031-
955   0182(97)00014-X, 1997.

Poulton, A. J., Stinchcombe, M. C., Achterberg, E. P., Bakker, D. C. E., Dumousseaud, C., Lawson, H. E., Lee, G. A., Richier, S., Suggett, D. J. and Young, J. R.: Coccolithophores on the north-west European shelf: Calcification rates and environmental controls, Biogeosciences, 11(14), 3919–3940, doi:10.5194/bg-11-3919-2014, 2014.

Ridgway, K. R. and Condie, S. A.: The 5500-km-long boundary flow off western and southern Australia, J. Geophys. Res. C
960   Ocean., 109(4), 1–18, doi:10.1029/2003JC001921, 2004.

Ridgway, K. R. and Godfrey, J. S.: The source of the Leeuwin Current seasonality, J. Geophys. Res. Ocean., 120(10), 6843–6864, doi:10.1002/2015JC011049.Received, 2015.

Shannon, C. E.: A Mathematical Theory of Communication, Bell Syst. Tech. J., 27(3), 379–423, doi:10.1002/j.1538-7305.1948.tb01338.x, 1948.

965   Sharples, J., Moore, C. M., Hickman, A. E., Holligan, P. M., Tweddle, J. F., Palmer, M. R. and Simpson, J. H.: Internal tidal mixing as a control on continental margin ecosystems, Geophys. Res. Lett., 36(23), 1–5, doi:10.1029/2009GL040683, 2009.

Smith, M., De Deckker, P., Rogers, J., Brocks, J., Hope, J., Schmidt, S., Lopes dos Santos, R. and Schouten, S.: Comparison of U37K', TEX86H and LDI temperature proxies for reconstruction of south-east Australian ocean temperatures, Org. Geochem., 64, 94–104, doi:10.1016/j.orggeochem.2013.08.015, 2013.

970   Smith, R. A., Castañeda, I. S., Groeneveld, J., De Vleeschouwer, D., Henderiks, J., Christensen, B. A., Renema, W., Auer, G., Bogus, K., Gallagher, S. J. and Fulthorpe, C. S.: Plio-Pleistocene Indonesian Throughflow Variability Drove Eastern Indian Ocean Sea Surface Temperatures, Paleoceanogr. Paleoclimatology, 35(10), 1–20, doi:10.1029/2020PA003872, 2020.

Stuut, J.-B. W., De Deckker, P., Saavedra-Pellitero, M., Bassinot, F., Drury, A. J., Walczak, M. H., Nagashima, K., and Murayama, M.: A 5.3-million-year history of monsoonal precipitation in northwestern Australia. Geophys. Res. Lett., 46,
975   6946– 6954, doi:10.1029/2019GL083035, 2020.

Suchéras-Marx, B., Escarguel, G., Ferreira, J. and Hammer, Ø.: Statistical confidence intervals for relative abundances and abundance-based ratios: Simple practical solutions for an old overlooked question, Mar. Micropaleontol., 151, doi:10.1016/j.marmicro.2019.101751, 2019.

980 Takahashi, K. and Okada, H.: The paleoceanography for the last 30,000 years in the Southeastern Indian Ocean by means of calcareous nannofossils, Mar. Micropaleontol., 40(1–2), 83–103, doi:10.1016/S0377-8398(00)00033-5, 2000.

Thierstein, H. R. and Young, J. R. (Eds): Coccolithophores: From Molecular Processes to Global Impact, 565 pages, Springer, Berlin, Heidelberg., doi:10.1007/978-3-662-06278-4, 2004.

Thompson, P. A., Pesant, S. and Waite, A. M.: Contrasting the vertical differences in the phytoplankton biology of a dipole pair of eddies in the south-eastern Indian Ocean, Deep. Res. Part II Top. Stud. Oceanogr., 54(8–10), 1003–1028, 985 doi:10.1016/j.dsr2.2006.12.009, 2007.

Thompson, P. A., Wild-Allen, K., Lourey, M., Rousseaux, C., Waite, A. M., Feng, M. and Beckley, L. E.: Nutrients in an oligotrophic boundary current: Evidence of a new role for the Leeuwin Current, Prog. Oceanogr., 91(4), 345–359, doi:10.1016/j.pocean.2011.02.011, 2011.

van der Weijst, C. M. H., van der Laan, K. J., Peterse, F., Reichart, G.-J., Sangiorgi, F., Schouten, S., Veenstra, T. J. T., and 990 Sluijs, A.: A 15-million-year surface- and subsurface-integrated TEX$_{86}$ temperature record from the eastern equatorial Atlantic, Clim. Past, 18, 1947–1962, https://doi.org/10.5194/cp-18-1947-2022, 2022.

Van Oostende, N., Harlay, J., Vanelslander, B., Chou, L., Vyverman, W. and Sabbe, K.: Phytoplankton community dynamics during late spring coccolithophore blooms at the continental margin of the Celtic Sea (North East Atlantic, 2006–2008), Progress in Oceanography, Prog. Oceanogr., 104, 1–16, doi:10.1016/j.pocean.2012.04.016, 2012.

995 Wade, B. S. and Bown, P. R.: Calcareous nannofossils in extreme environments: The Messinian Salinity Crisis, Polemi Basin, Cyprus, Palaeogeogr. Palaeoclimatol. Palaeoecol., 233(3–4), 271–286, doi:10.1016/j.palaeo.2005.10.007, 2006.

Wara, M. W., Ravelo, A. C. and Delaney, M. L.: Climate change: Permanent El Niño-like conditions during the Pliocene warm period, Science (80-.)., 309(5735), 758–761, doi:10.1126/science.1112596, 2005.

Young, J.: Size variation of Neogene *Reticulofenestra* coccoliths from Indian Ocean DSDP Cores, J. Micropalaeontology, 1000 9(1), 71–85, doi:10.1144/jm.9.1.71, 1990.